Heling, Laurens Wilhelmus Hubrecht Joseph (2019) ***Biochemical Mapping of Myofibrillar ATPase using STORM Imaging.*** **Master of Science by Research (MScRes) thesis, University of Kent,.**

Biochemical Mapping of Myofibrillar ATPase using STORM Imaging

Laurens Heling

A Thesis submitted to the University of Kent for the degree of

Master of Science in Biochemistry

August 2019

Supervisors: Dr Neil M. Kad and Professor Michael A. Geeves

Department of Biosciences

Declaration

No part of this thesis has been submitted in support of an application for any degree or qualification of the University of Kent or any other University or institute of learning.

Laurens Heling

August 2019

Acknowledgements

I would like to express my gratitude to the members of the Kad and Geeves laboratories who have engaged in useful discussions and assisted me getting a grasp of various techniques.

On a more personal note I would like to thank the people that have been vital for the completion of this work. My parents, brother, sister and family for their support, listening ear and guidance. My lab mates Jamie and Rob for the spontaneous pub visits and introducing me to a whole new side of Canterbury. My best friends Jochem, Yoella, Leoni, Lukas, Nikki, Enea, Sheyla, Myrto, Lulu and Rosalba for making me feel at home wherever I was; the many days and nights of fun, food, drinks, lots of coffee and the most interesting conversations.

My supervisors Mike and Neil were fundamental for this work. Their enthusiasm and guidance through the trials and tribulations of this project has been inspirational. Their support has given me the confidence to bring up my own ideas and discuss on a higher academic level. The ability to work out details of experiments while always keeping an eye on the bigger scientific question taught me a great deal what it is like to do science, and how to have fun with it. Without their involvement I think I would not have chosen to continue my career in research.

Abstract

The study of muscle contraction has led to a good understanding of this complex and highly regulated process. Small changes as a result of trauma or mutations can have catastrophic downstream effects. Bulk kinetics have shown that relaxed muscle myosin exists in two subpopulations, the Disordered RelaXed State (DRX) and the severely inhibited Super RelaXed State (SRX) with 5-100-fold slower ATP hydrolysis rates. Mutations in the potential regulators of the SRX have been extensively linked with Hypertrophic Cardiomyopathy (HCM). The spatial arrangement of the SRX within the sarcomere however is unknown. To better understand what components play a role in the SRX, a spatiotemporal image is necessary. Here we recorded single fluorescent ATP molecules binding and releasing from myosin in single myofibrils. First, we showed the structural reconstruction of the myofibril using super resolution Stochastic Optical Reconstruction Microscopy (STORM) which indicated that most ATP bind at the A-band. Next, we calculated the spatiotemporal arrangement of the ATP which showed that there are two distinct populations in the sarcomere with different rates. Mapping each individual binding event suggested that the populations with longer lifetimes reside mainly in the C-zone, however the use of structural markers must conclude this. The dissociation kinetics were well fit to a double exponential, yielding a minimum 5-fold increase in the ATP lifetime of the second population. The rates we observed are faster than what has previously been reported. This may be due to several factors that can be resolved in future experiments. We conclude that the methods laid out here are sensitive enough to measure and calculate the dissociation rate of single ATP molecules with myosin. The results obtained are important for further development of this assay which may help clarify the components that play a role in SRX and promote the development of new therapeutics against cardiovascular diseases like HCM.

Table of Contents

List of Figures and Tables

Figures

Tables

Abbreviations

Å	Angstrom
ADP	Adenosine Diphosphate
ATP	Adenosine Triphosphate
BMR	Basal Metabolic Rate
Ca^{2+}	Calcium Ion
CaMKII	Ca^{2+}/calmodulin-dependent protein kinase
DCM	Dilated Cardiomyopathy
DRX	Disordered-Relaxed State
EGTA	Ethylene glycol-bis(β-aminoethyl ether)-N,N,N′,N′-tetraacetic acid
ELC	Essential Light Chain
EM	Electron Microscopy
HCM	Hypertrophic Cardiomyopathy
HMM	Heavy Meromyosin
IHM	Interacting Heads Motif
k	Rate Constant
LMM	Light Meromyosin
MLCK	Myosin Light Chain Kinase
MOPS	3-(N-morpholino) propanesulfonic acid
MyBP-C	Myosin Binding Protein C
OAF	Oblique angle fluorescence
P_i	Inorganic Phosphate
PKA	Protein Kinase A
PKC	Protein Kinase C
PKD	Protein Kinase D
prox S2	Proximal S2
RLC	Regulatory Light Chain
RPM	Revolutions Per Minute
S1	Subfragment-1 of Myosin
S2	Subfragment-2 of Myosin
SRX	Super-Relaxed State
STORM	Stochastic Optical Reconstruction Microscopy
Tm	Tropomyosin
TnC	Troponin C
TnI	Troponin I
TnT	Troponin T
WT	Wild Type

1. Introduction

Motion is the basis of animal life, and the study of the main contributor to motion: muscle, has been of scientific interest for centuries. How can a highly organised molecular machine convert chemical energy into mechanical motion with such high efficiency? Over the last 150 years, since myosin was identified as the protein in muscle that drives contraction (Kühne, 1864), knowledge has grown extensively on how this molecular machine works. During the 1930s and 40s the understanding of muscle biochemistry was elucidated, with actin identified as a major binding partner and ATP through ATP hydrolysis as the fuel for contraction (Szent-Györgyi, 1951). In the following decades the mechanical and structural organisation of muscle proteins in interdigitating thick and thin filaments (Huxley, 1953a; Huxley and Niedergerke, 1954; Huxley and Hanson, 1954) was resolved. This cumulated in the development of the swinging lever arm theory during the 1950s and 1960s (Huxley, 1969). *In vitro* motility assays with purified and recombinant proteins performed from the 1980s onward supported this theory and showed that this process is driven by the cyclic interaction between myosin subfragment-1 (S1) and actin filaments coupled with ATP hydrolysis and conformational changes of the myosin heads (Kron and Spudich, 1986; Toyoshima *et al.*, 1987; Finer *et al.*, 1994; Geeves and Holmes, 1999). There is now a good, albeit not complete, understanding of the role and function of the most important sarcomeric proteins during muscle contraction.

1.1 The Myosin Crossbridge Cycle

The actin activated chemo-mechanical cycle of myosin S1 is a multistep cycle of interactions that through conformational and enzymatic changes in the myosin motor domain ultimately lead to the sliding of the actin filament along the myosin filament. This model was first proposed in 1971 (Lymn and Taylor, 1971). Myosin can bind and hydrolyse ATP to ADP on its own, albeit very slow. Actin, acting as a competitor to ATP, activates the myosin crossbridge cycle. The cycle (**figure 1.1**) starts with a pre-stroke S1 with ADP and inorganic phosphate (P_i) bound to the nucleotide site, binding to actin. The release of the P_i and the power stroke follows, which swings the lever arm to the right, and the converter domain bends through an angle of 70°, to the post-stroke position. This slides the actin filament to the left. Next, the ADP is released, freeing the nucleotide site for ATP which weakens the binding affinity of S1 to actin. ATP hydrolysis converts the heads back into the pre-stroke position.

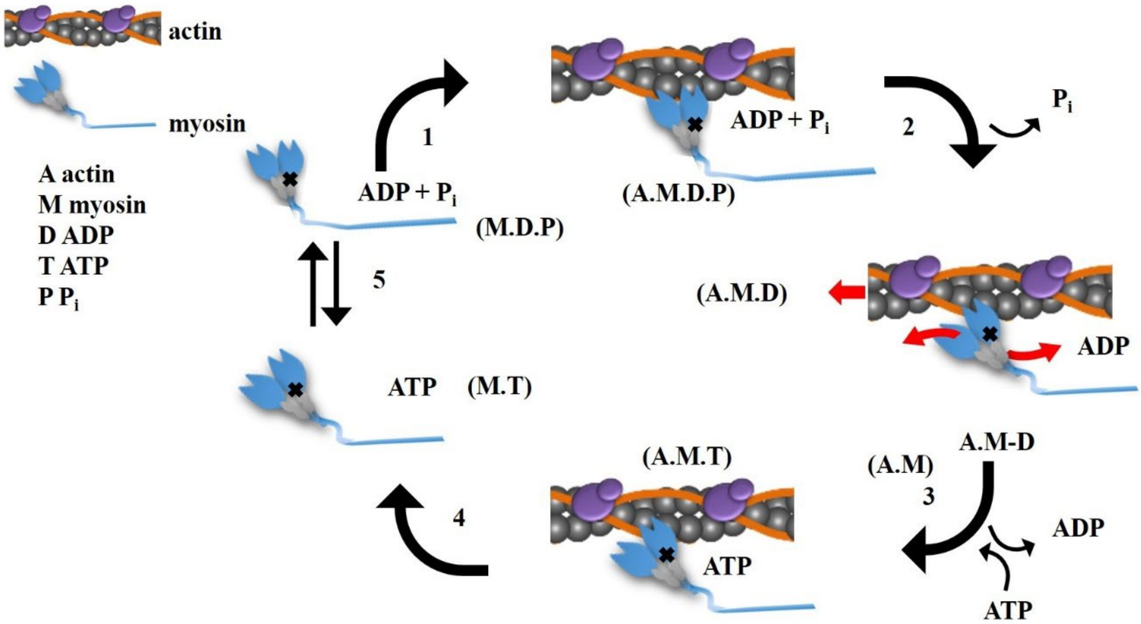

Figure 1.1 Simplified diagram of the actin activated crossbridge cycle. The steps in the chemo-mechanical cycle are: **1** Myosin motor domain S1 in the pre-stroke position with ADP and inorganic phosphate P_1 at the nucleotide site binds to actin. **2** P_i is released and the lever arm of S1 goes through a conformational transition, swinging to the right in relation to the converter domain (indicated by the black cross) to perform the power stroke. The movements of the components in relation to the thick filament is shown by the red arrows. **3** The binding affinity of ADP decreases and ADP is released, vacating the nucleotide site for ATP binding. **4** ATP releases the myosin from the actin filament. **5** ATP hydrolysis transitions the myosin back to the pre-stroke position. Figure adapted from (Ujfalusi *et al.*, 2018)

1.2 The Sarcomere

Three types of muscle exist. Smooth muscles line the blood vessels and is found on the walls of organs, cardiac muscle is responsible for pumping blood around the body and skeletal muscle is responsible for multiple aspects including posture and motion. Skeletal and cardiac muscles, when viewed under the microscope show striations perpendicular to the axis caused by the sarcomere, a highly regularly organised structure of interdigitating thick and thin filaments (Huxley, 1953b; Huxley, 1957). Sarcomeres are the serially organised end-to-end in myofibrils which bundled up form a muscle fibre. Muscle contraction is the results of the concerted shortening of thousands of sarcomeres. This makes the sarcomere an ideal system to study. The lateral boundaries of each sarcomere are the Z-line. The Z-line, from the German Zweischenscheibe literally meaning disk in between, is a protein dense disk which anchors the barbered end of the actin filaments of adjacent sarcomeres through interactions with CapZ and α-actinin (Maruyama and Ebashi, 1965). Traditionally thought to be merely a passive structural component, Z-disk proteins and their associated networks have been shown to regulate a multitude of cellular processes in striated muscles (Luther, 2009; Burgoyne *et al.*, 2015) and mutations in Z-disk proteins have been linked with cardiomyopathies (Knöll *et al.*, 2011). The I-band is on either side of the Z-line and is lacking any myosin. During contraction the I-band is the only structure in the sarcomere to change its length as it contains the spring-like elements of titin. The I-band is further more important in providing the stiffness and elasticity during diastole (Trinick, 1996; Freundt and Linke, 2019). The A-band is nearly entirely comprised of the interdigitating filaments, apart from the H-zone which contains only thick filaments. Within the H-band lie the M-line and the P-zones, where actin is absent. The M-line, from the German Mittelscheibe literally meaning middle disk, is another multiprotein structure that is responsible for regulating a variety of processes. The M-line is responsible for crosslinking myosin, through myomesin, which stabilizes myosin at the centre of the sarcomere during contraction, as well as playing an important role in actin dynamics, proteasomal degradation and signal transduction (Hu *et al.*, 2015; Lange *et al.*, 2019).

Mutations in M-line proteins have been linked to muscle dysfunction (Koebis *et al.*, 2011; Siegert *et al.*, 2011). See **figure 1.2** for a visual representation of the sarcomere

The A-band can be further divided up to the D-zone and the C-zone. The C-zone is where myosin binding protein-C is present, an accessory protein of the thick filament that has a possible role in maintaining the interacting heads motif (IHM) and the super relaxed state (SRX). These topics will be discussed in more detail later (1.3 and 1.4), but it is worth mentioning that the D-zones and C-zones are an important topic of this thesis as the location in the sarcomere where the SRX predominately exists may relate to these zones.

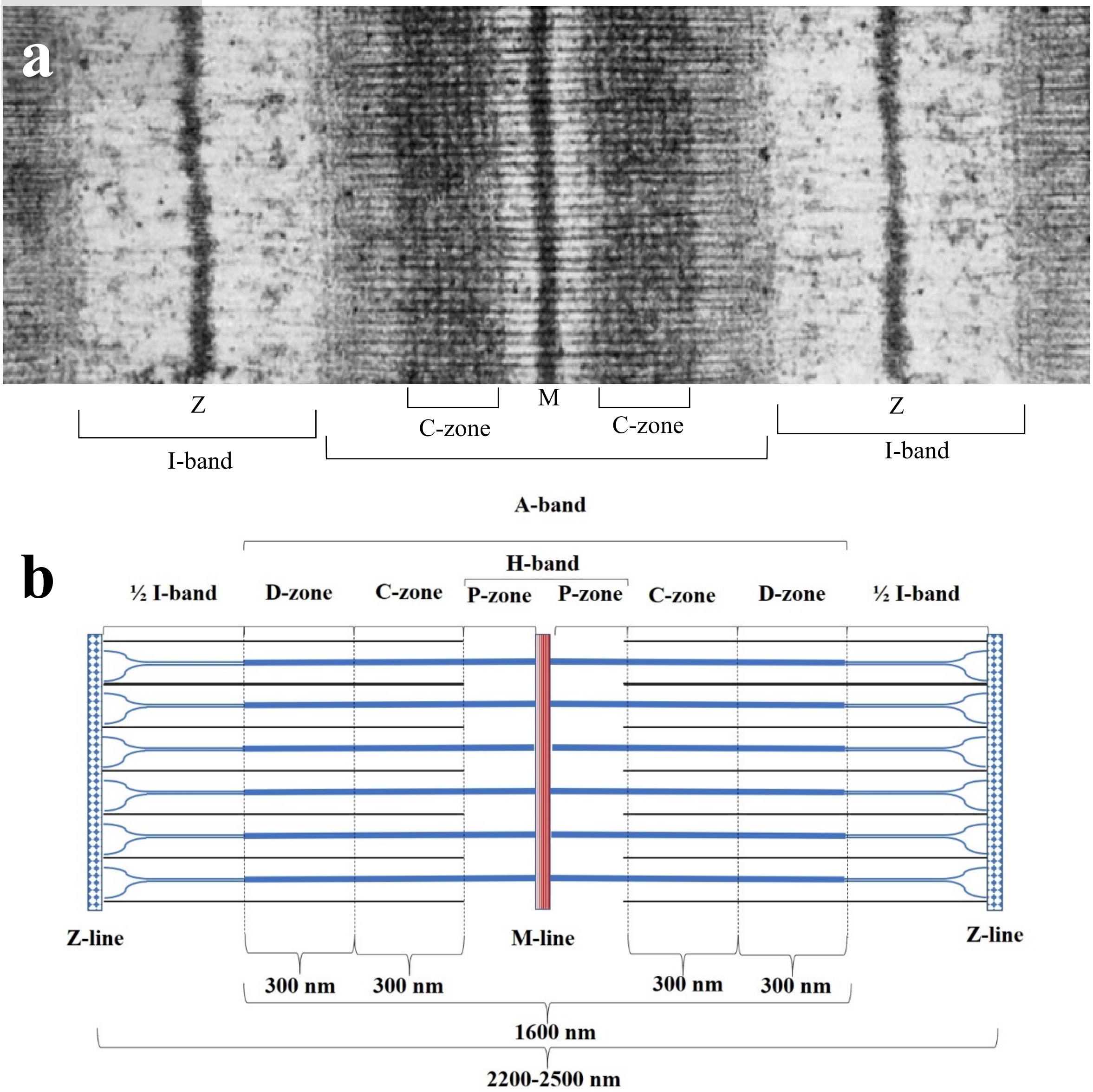

Figure 1.2 | The sarcomere. **(a)** Electron micrograph of a rabbit skeletal muscle sarcomere negatively stained for myosin binding protein C. The ultrastructure is clearly identifiable. **(b)** Schematic description of the sarcomere. The A-band in this diagram is the region where myosin exists. The A-band can be divided into the D-zones, C-zones, where actin myosin cross-bridges can occur and the P-zones which is unoccupied by actin. The P-zones fall within the H-band, which is divided in the middle by the M-line. Myosin is absent from the I-band, which divided in half by the Z-line. Sarcomeres in relaxing conditions are approximately 2.2-2.5 µm in length and the A-band is approximately 1.6 µm in length. The D and C zone are approximately 300 nm in length. Figure in panel **(a)** is adapted from (Craig and Offer, 1976)

1.2.1 The Thin Filament, Actin and the Steric Blocking Model

Actin monomers, the most abundant protein in cells formed of four compact domains, form the core of the thin filament in a single start helical structure with an axial periodicity of approximately 400 Å (Selby and Bear, 1956). Coiled-coil tropomyosin, a 40 nm long protein that stretches continuous over 7 actin monomers and first found actin binding partner (Bailey, 1946; Bailey, 1948) was the inspiration for the Hanson and Lowy model that tropomyosin sterically regulates myosin cross bridge binding to actin and thus muscle contraction (Hanson and Lowy, 1964). This formed the basis for the hypothesis that tropomyosin reacts to Ca^{2+} by moving across the thin filament azimuthally that blocks and unblocks the myosin binding sites and thus determine contraction and relaxation (Huxley, 1971; Haselgrove, 1973; Parry and Squire, 1973). Later it was shown that a third component, the troponin complex formed of equimolar amounts of troponin C (TnC), troponin T (TnT) and troponin I (TnI), was responsible for the thin filament's Ca^{2+} response by acting as a Ca^{2+} specific receptor (Ebashi, 1963; Ebashi and Endo, 1968; Ebashi *et al.*, 1969). One troponin complex binds to one tropomyosin along the thin filament (Hanson, 1967; Potter, 1974). Thus, the thin filament is a repeating structure of actin$_7$·TmTn. The calcium dependent shifts of tropomyosin are the mechanistic basis of thin filament controlled muscle activation and have been structurally (Vibert *et al.*, 1997; Poole *et al.*, 2006) and functionally (Lehrer and Morris, 1982; Ngai *et al.*, 1986; Mckillop and Geeves, 1993) formalized to exist in the three states according to the McKillop-Geeves model (Mckillop and Geeves, 1993): open – where myosin S1 is unhindered to binding the thin filament; closed – where weak binding is possible; and blocked – where tropomyosin prevents any binding of S1. Later called the M-, C- and B-states to avoid confusion (myosin was still able to bind actin while in the "closed" state), this model is still in current use **(Figure 1.3)**. The model states that Ca^{2+} binding to troponin is not enough to completely stimulate the actomyosin interactions. Low [Ca^{2+}]-B and high [Ca^{2+}]-C confirmations of the thin filament do no stimulate myosin ATPase, and the M-state is activated when both myosin and Ca^{2+} are bound to the TmTn regulated thin filaments. The C-state can thus be regarded as a transition state between the B- and M-states. The model further states a cooperative binding pattern in the C-state, where a myosin head bound to actin leaves space for adjacent free myosin heads to access unoccupied actin (Kad *et al.*, 2005). The interaction of the free heads causes a transition from the C- to the M-state.

Thin filament regulation is one of the primary methods by which muscle contraction can be regulated, but secondary mechanisms have emerged that added serious complexity to the beat-to-beat regulation. These secondary regulatory mechanisms are thick filament associated and offer new areas of research.

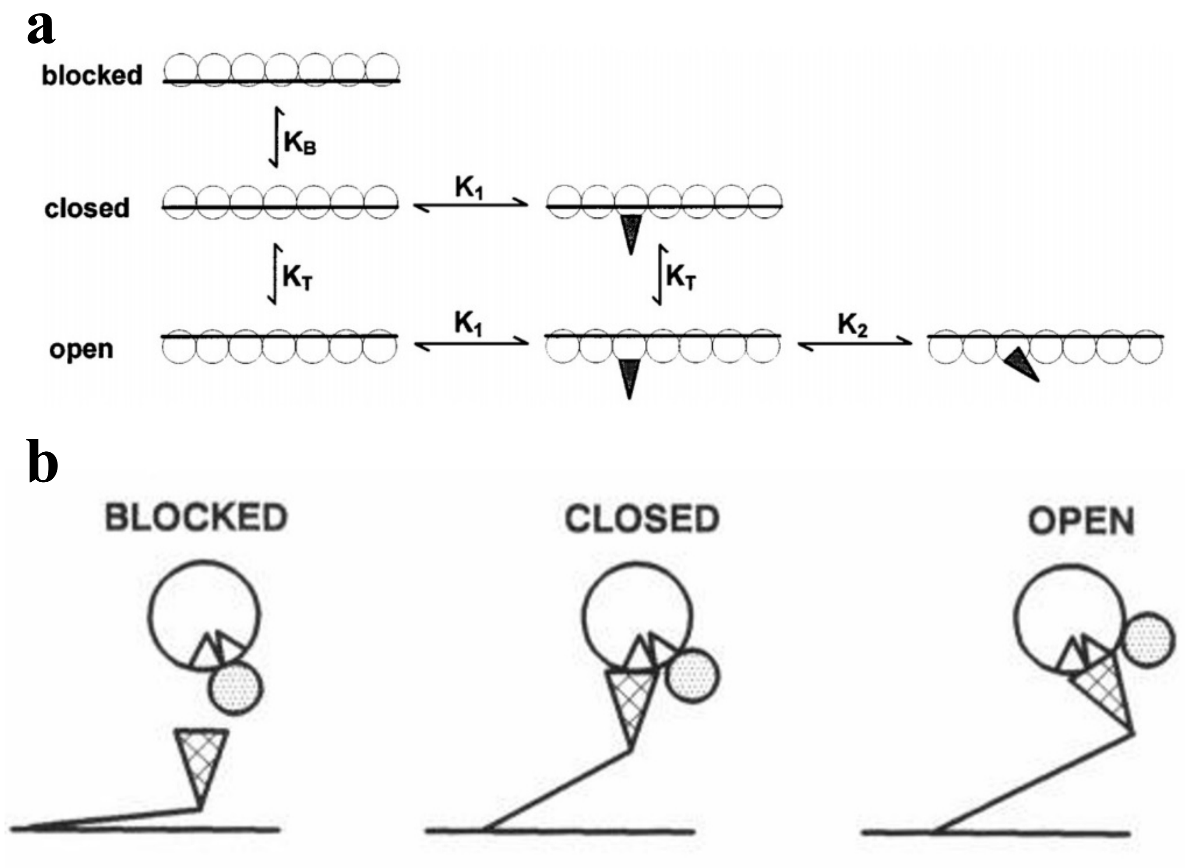

Figure 1.3 | The McKillop-Geeves Three State Model of Thin Filament regulation.

In the blocked B state of the steric blocking model S1 is hindered of binding, where the closed C confirmation does allow weak binding of the myosin. Contraction is only possible in the open M confirmation. Myosin bound to actin in the C-state configuration may be able to displace tropomyosin to expose myosin binding sites and result in a cooperative activation of the thin filament. (**a**) Blocked, closed and open states schematically described. Tropomyosin-troponin complexes are show by a horizontal black line running over 7 open circles representing the actin repeats. Myosin is shown by a black triangle. The equilibriums K_{B} and K_{T} are calcium sensitive. **(b)** Schematic description of the same model as above, with myosin depicted by crossed triangles, and tropomyosin as dotted circles, showing the azimuthal movement between the states. Figure in panel **(a)** adapted from (Maytum *et al.*, 1999). Figure in panel **(b)** adapted from (Mckillop and Geeves, 1993).

1.2.2 The Thick Filament, Myosin and the IHM

The major component of the thick filament is myosin. Muscle myosin is a hexamer protein that consists of two myosin heavy chains, and two sets of myosin light chains (the essential light chain (ELC) and the regulatory light chain (RLC)) **(figure 1.4a**). Proteolytically digestion of myosin molecules by α-chymotrypsin yields two fragments namely heavy meromyosin (HMM) and light meromyosin (LMM). HMM yields subfragment-1 (S1) with its actin and ATP binding site, subfragment-2 (S2). The LMM interacts with LMM regions of adjacent myosin molecules to form a cylindrical backbone with projecting myosin crowns rotated 40° around the thick filament 14.3 nm apart with a 42.9 nm true repeat along the length of the filament.

The S1 domain **(figure 1.4b)** contains the nucleotide and actin binding sites as well as the converter domains that can swing through an angle of ~70° when transitioning between the pre- and post-stroke states during contraction (described in **section 1.1**) S1 further contains the recently characterised myosin "mesa", a flat surface at a steep angle from the actin binding sites that is highly conserved in cardiac myosin and a hotspot for mutations that cause hypertrophic cardiomyopathy (HCM; discussed in more detail in **section 1.3**) (Nag *et al.*, 2017) **(Figure 1.4c)**. Additionally, S1 contains the RLC and ELC domains. The RLC is a small protein that stabilises the neck region of myosin together with the ELC. The sliding velocity of actin along the thick filament is linked to the ELC and RLC, essential for the conversion of chemical energy into mechanical motion (Lowey *et al.*, 1993). The RLC can be phosphorylated which is an important regulator of the force and velocity of contraction and activates sarcomere contraction which is explained in more detail below.

Another member of the thick filament proteins is titin, the largest known protein that spans half the sarcomere from the Z-line to the M-line and fulfils distinct roles in all regions of the sarcomere. The extendible I-band portion of titin modulates the stiffness of the sarcomere by acting as a molecular spring through passive force. The thick filament bound part of titin contains a series of repeats and super repeats of IgI and FnIII that regulate the length of the thick filament as well as being an anchor for accessory proteins. The larger super repeat of this region follows the same true 42.9 nm periodicity as myosin.

Furthermore, the thick filament hosts Myosin binding protein C (MyBP-C), which will be discussed in more detail in **section 1.4.1**.

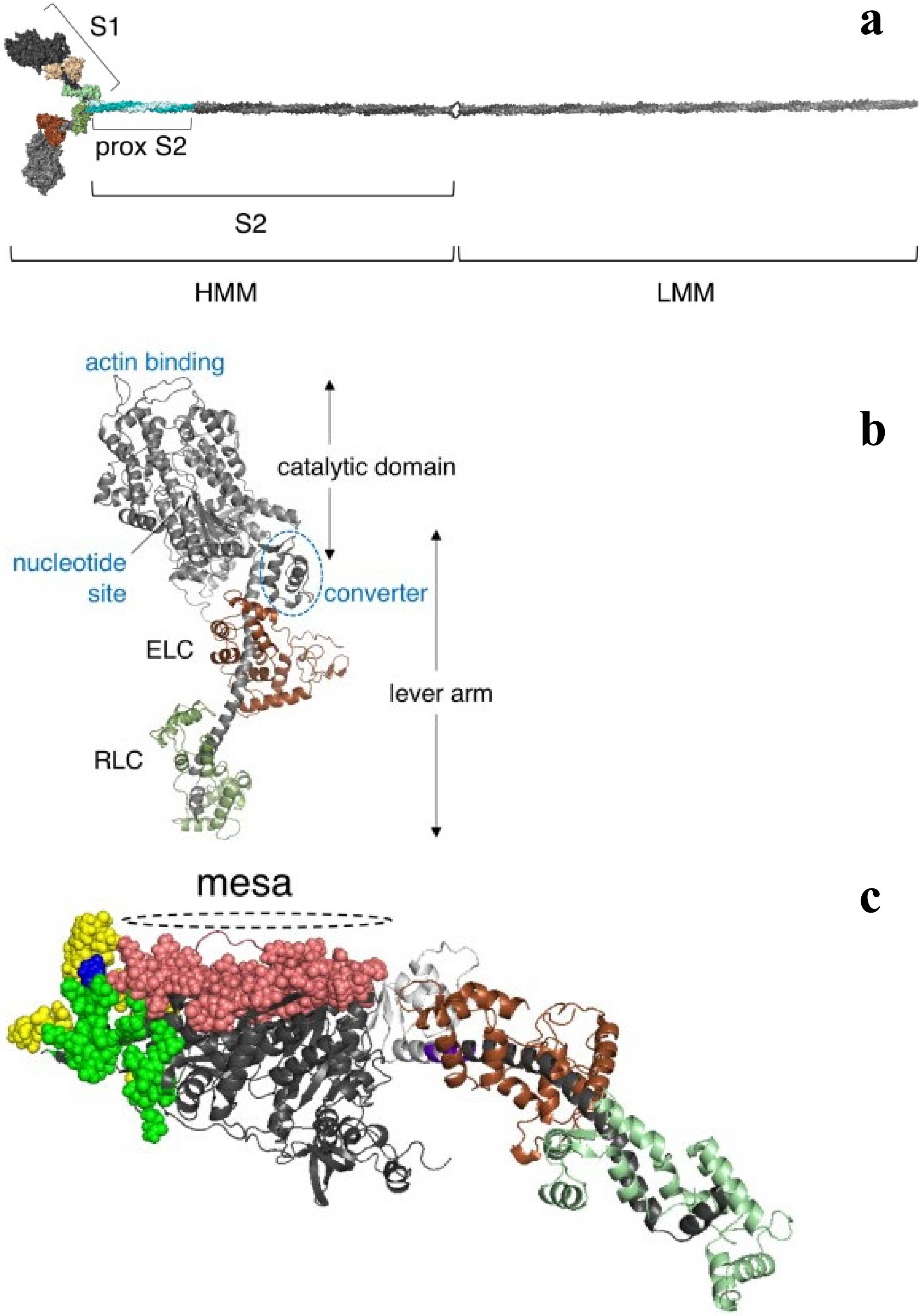

Figure 1.4 | Structure of Human β cardiac Myosin

(a) Homology model of β cardiac myosin rendered in PyMOL. **(b)** Homology model myosin S1 with the neck region - ELC and RLC, and the catalytic domain with the actin binding site and the nucleotide binding site rendered in PyMOL. **(c)** Side view of structural model of S1 in the pre-stroke state showing the myosin mesa region in pink, with the neighbouring actin binding site in yellow and nucleotide binding site in green. These three surfaces form a pyramid like structure with arginine at its vertex that is a known mutation spot. The ribbon components have the same colour as in **(b).** Figures in all panels are adapted from (Trivedi *et al.*, 2017)

Studies on intact thick filaments have shown a folding state of myosin favoured by intramolecular interactions and intermolecular interaction with neighbouring S1 heads (Woodhead *et al.*, 2005; Zoghbi *et al.*, 2008; Zhao *et al.*, 2009) bent backwards against the thick filament. The intermolecular folded state of myosin was later coined the interacting heads motif (IHM) (Alamo *et al.*, 2008), where the binding surface of one myosin head (the blocked head, because the actin-binding site is unavailable in the folder state) binds to the converter domain of another myosin head (the free head, where the actin-binding site is not sequestered) **(See figure 1.4c and 1.5)**. The mesa regions of both heads cradle the prox. S2 region. This IHM structure has been shown to exist in a wide variety of muscles across species. The domains that are involved in the IHM structural state are also known to be hotspots for HCM mutations (Table 1). Heads in the IHM are prevented to participate in the chemo-mechanical cycle, reducing the power output of muscle as well as inhibiting ATPase activity of the free head. Mutations that disrupt this structural state can therefor lead to an increased ATPase activity and power output. The inter and intramolecular interactions in the IHM are believed to be the structural basis for the inhibited ATP turnover that is observed in the super-relaxed state of myosin (the SRX; discussed in **section 1.4**).

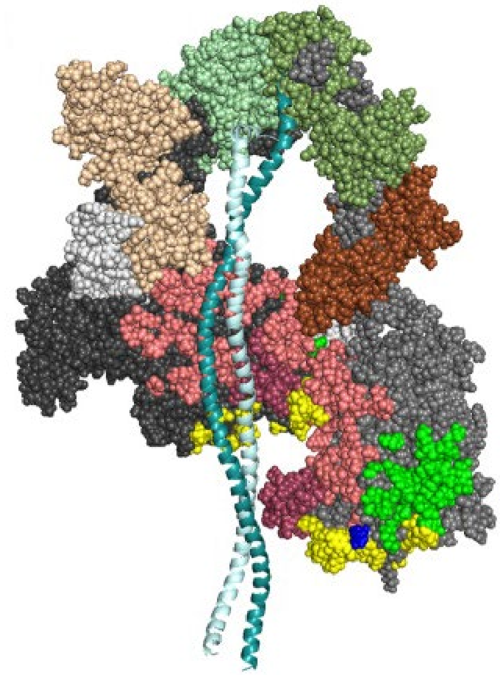

Figure 1.5 | Model of Interacting Heads Motif Structural model of the off state of the IHM. This model was based on the 3 dimensional reconstruction of Tarantula thick filaments (Alamo *et al.*, 2016). Colour used are similar to the colours in **figure 1.4** Figure adapted from (Trivedi *et al.*, 2017)

1.3 Cardiomyopathies

Cardiomyopathies are a collection of disorders of which the most common are hypertrophic cardiomyopathy (HCM), dilated cardiomyopathy (DCM) and arrhythmogenic right ventricular cardiomyopathy (ARVC), three congenital myopathies. The first mutation linked to cardiomyopathy was the single point mutation R403Q in the human β myosin heavy chain (MHC) in 1990, causing familial hypertrophic cardiomyopathy (Geisterfer-Lowrance, A.A., Kass, S., Tanigawa, G., Vosberg, H.P., McKenna, W., Seidman, C.E., Seidman, 1990). Since then more than 300 mutations have been mapped to the β-MHC gene (Seidman and Seidman, 2001; Buvoli *et al.*, 2008; Walsh *et al.*, 2009; Colegrave and Peckham, 2014; Homburger *et al.*, 2016), mainly within the motor domain, that lead to HCM. This has caused a shift of focus in muscle research towards a better understanding of the molecular basis of cardiomyopathies.

1.3.1 Hypertrophic Cardiomyopathy

Hypertrophic cardiomyopathy is the most common form of inherited heart disease, affecting 1 in 200 people and the leading cause of sudden death in seemingly healthy individuals under 35 years of age. (McKenna and Behr, 2002; Harvey and Leinwand, 2011; Maron *et al.*, 2013; Semsarian *et al.*, 2015). HCM is characterised by an asymmetrical hypertrophy of the ventricular wall while generally preserving the volume of heart muscle, resulting in a decreased ventricular chamber size. While force output during systole is preserved, the diastolic capacity is severely reduced (Towbin, 2009). This leads to hyper-contractibility, one of the clinical symptoms of HCM.

Mutations that cause HCM are linked directly to sarcomeric proteins, with ~35% of the mutations mapped to human β cardiac myosin, causing mainly missense mutations (Colegrave and Peckham, 2014), and ~35% to cardiac (c)MyBP-C, leading to a truncation of the protein (Harris *et al.*, 2011). But how mutations in these proteins lead to clinical hyper-contractibility on a molecular level remain unclear. Results of studies of the last 15 years on these mutations do not explain the changed biochemical and biophysical output of myosin. One hypothesis is that HCM mutations cause an increase of the power output by altering one or more parameters. Power output is determined by the velocity of the actin thin filament sliding across the collective of myosin motors producing force during contraction. This relationship can be estimated using equation (1):

$$F_{collective} = F_{intrinsic} \times N_a \times duty\ ratio \qquad (1)$$

where $F_{intrinsic}$ is the force of a single myosin motor domain, N_a is the number of myosin heads that can functionally access the actin thin filament and *duty ratio* is the fraction of accessible heads strongly bound to actin at any time during contraction.

Myosin Mesa	Blocked Head Converter Binding Domain	Converter Domain	Proximal S2	
R169G	I303M	G716R	S842G	E894G
R249N	D382Y	R719W	K847E	D906G
H251N		R723C	E848G	L908V
I263T		I730M	R858S	L908Q
R403Q		P731S	R858P	I909M
R442C		G733E	R858C	E924K
N444S		Q734P	K865R	D928V
R453C		I736T	R869H	E930Q
I530V		G741R	R870H	
E603K		F764Y	E875del	
V606M		G768R	M877I	
G607D			V878A	
R652G			Q882E	
R663H			N885K	

Table 1 | HCM mutations in myosin mesa, blocked head converter binding domain, converter domain and Prox. S2 Residues identified as HCM mutations (Homburger *et al.*, 2016) that lie on the domains involved in the IHM. Colours correspond with **figure 1.4c**. Adapted from (Trivedi *et al.*, 2017)

Increases to any of these parameters will cause an increase in force and thus hyper-contractility. Studies in determining the parameters affected in HCM yielded contrasting results. Early onset HCM mutations on recombinant β cardiac myosin showed a significant increase of force, velocity and ATPase activity, while the same experiments with adult onset

HCM mutations showed modest to no change compared to wild type (WT) (Sommese *et al.*, 2013; Nag *et al.*, 2015; Adhikari *et al.*, 2016; Kawana *et al.*, 2017) some of which contributed to hyper-contractility while hypo-contractility was also observed.. N_a does not entail all the myosin heads present in the sarcomere. Only a fraction of those, that may be as low as 50%, is functionally able to bind actin (Brito *et al.*, 2011), while the rest of myosin heads is sequestered in the interacting heads motif (IHM) through its myosin mesa and blocked head converter binding domains to an off-state of myosin hydrolysis termed the super-relaxed state (SRX). The number of myosin heads available to functionally access actin may be the link between HCM mutations and clinical hyper-contractility.

1.4 The Super Relaxed State of Myosin

ATP hydrolysis by myosin in striated muscle exists in three states. The active cycling state, where myosin and actin interact, regulated by [Ca^{2+}] through the steric blocking model (**section 1.2.1**), exhibits fast ATP turnover of generally less than 1s. Under relaxing conditions, with low or no Ca^{2+} present, the ATP turnover is divided in two subpopulations. The disordered-relaxed state (DRX), where myosin heads are not bound to actin, generally has an ATP turnover closer to 30s, similar to that of purified myosin, while the super-relaxed state (SRX) has a strongly inhibited ATP turnover of 150-300s (approximately 145 s in cardiac sarcomeres (Hooijman *et al.*, 2011)).

In the 1970s it was observed that there is an inconsistency between the metabolic rate of purified myosin and living muscle suggesting an inhibited state of myosin present *in vivo*. The ATP use of purified frog myosin in solution was 5-fold greater compared to the resting metabolic rate of the muscle it came from (Ferenczi *et al.*, 1978), which later was also observed in rabbit skeletal muscle (Myburgh *et al.*, 1995). The discovery of the SRX with an extremely low release of nucleotides in rabbit skeletal (Stewart *et al.*, 2010), cardiac (Hooijman *et al.*, 2011), tarantula skeletal (Naber *et al.*, 2011) and mouse cardiac muscles

(McNamara *et al.*, 2016) explained this inconsistency. A simple experiment was conducted, taking advantage of the known kinetics of the chemo-mechanical cycle combined with fluorescent ATP. Dissociation of the ADP from myosin would end any emission. The change in fluorescent intensity is therefore directly related to the OFF rate of nucleotides to myosin (Stewart *et al.*, 2010; Hooijman *et al.*, 2011; Naber *et al.*, 2011).

The lifetimes of SRX in cardiac muscle are considerable slower than the SRX in skeletal muscle. SRX in skeletal muscle would be fully abolished upon partial activation of the fibres with Ca^{2+}, an effect that was not observed in cardiac muscle. The proportion of myosin in the SRX was comparable in fully relaxed and partially active conditions.

In skeletal muscle it was shown that myosin heads strongly bound to actin could induce stress in the thick filament that recruits myosin in the SRX to the DRX to make them accessible for contraction (Linari *et al.*, 2015). The necessity of this cooperative interaction between heads can be explained by the function of skeletal muscle, where upon activation it needs to generate instant force. Cardiac muscle, which must contract and relax consistently for a lifetime, is never fully activated under physiological conditions (Kobirumaki-Shimozawa *et al.*, 2014). To recruit all the myosin heads from the SRX every contraction would be energetically unfavourable. In cardiac muscle the SRX may play a cardioprotective role, managing energy expenditure and reserve myosin in the sequestered state in case of stress or differences to the load imposed by systemic circulation (Hooijman *et al.*, 2011; McNamara *et al.*, 2015).

The switch from DRX to the active state is controlled by the steric blocking model, while the SRX has several potential regulators described below.

1.4.1 Myosin Binding Protein-C

Myosin binding protein C (MyBP-C) is a sarcomeric accessory protein that was first identified in 1971 as contamination of crude skeletal muscle preparation (Starr and Offer, 1971). This multidomain protein is known in three isoforms, slow skeletal (ss), fast skeletal (fs) and cardiac (c), encoded by three separate genes (MYBPC1, MYBPC2 and MYBPC3) respectively. MyBP-C's location in the sarcomere is limited to the C-zones of the A-band, regularly patterned in 7-9 transverse parallel stripes approximately 43 nm apart, which corresponds with the true axial repeat of myosins along the thick filament. The protein is a linear polymer approximately 40 nm in length, 3 nm in width and with a molecular weight of ~140 kDa. Structurally MyBP-C consists of a series of subdomains that belong to the immunoglobulin or fibronectin type-III family depicted as C1-C10 from the N-terminus and a MyBP-C motif (or M-domain) linking C1 and C2 and a proline alanine rich (P/A) region at the N-terminus **FIG2a**. cMyBP-C has an additional immunoglobulin domain (C0) at the N-terminus and 4 serine residues in the M-domain that can be phosphorylated (Yasuda *et al.*, 1995) as well as an additional 28 amino acid loop in the C5 domain (Flashman *et al.*, 2004) **FIG2b**. MyBP-C is highly phosphorylated under baseline conditions, controlled by a diversity of protein kinases including PKA, PKC, PKD and CaMKII (Gautel *et al.*, 1995; Mohamed *et al.*, 1998; Bardswell *et al.*, 2010). Phosphorylation is severely reduced in cardiac conditions like HCM (Sadayappan *et al.*, 2005), supporting the physiological importance of MyBP-C phosphorylation. Due to the abundance of adrenergic targets in the sarcomere it is difficult to distinguish the precise functional effects, and thus our knowledge, of MyBP-C phosphorylation.

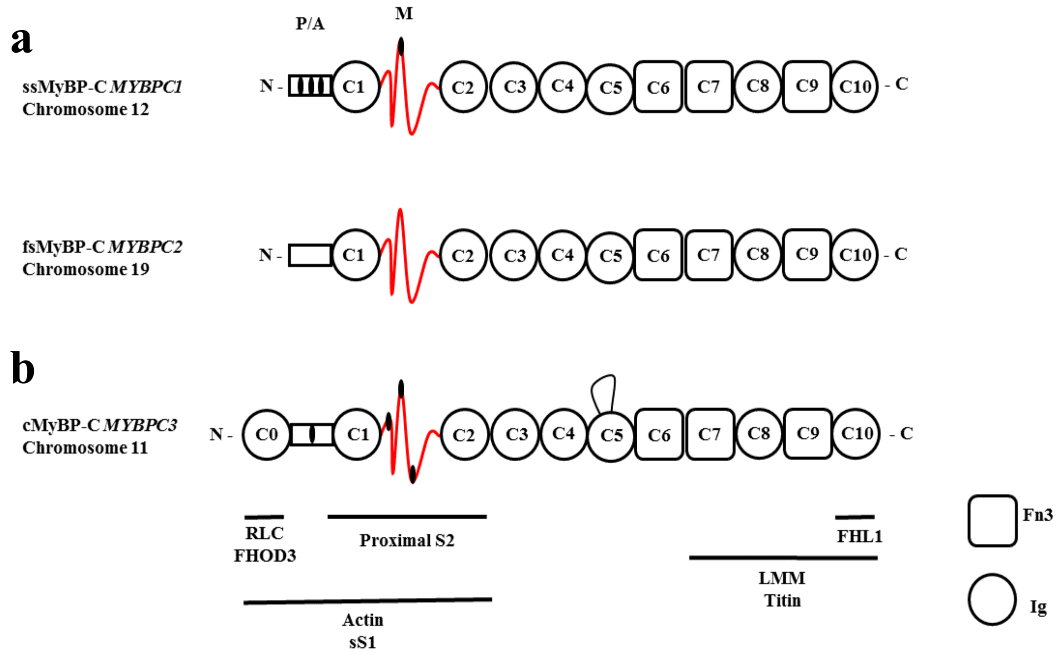

Figure 1.6 | Schematic diagram of MyBP-C paralogs. Full length domain organisation of slow skeletal, fast skeletal and cardiac MyBP-C. The known binding partners and binding positions are indicated by the stripes parallel to the axis below the diagram. **(a)** Full length ssMyBP-C and fsMyBP-C as well as the genes that encode them and chromosomal location. **(b)** Full length cMyBP-C with the gene that encodes it and the chromosomal location. cMyBP-C has an additional C0 Ig domain at its N-terminus as well as a 28 amino acid loop extending from C5. Note the phosphorylation sites in the P/A and M domain of the ssMyBP-C and cMyBP-C paralogs, indicated by small black ellipses. Figure from (Heling *et al.*, 2020).

MyBP-C is anchored to the thick filament through strong binding interactions between the C7-C10 domains and the LMM and titin. The remaining domains are thought to project from the thick filament to bind either the thick and thin filament (Luther *et al.*, 2011). The binding interaction of MyBP-C with actin was determined soon after its ability to bind myosin (Moos *et al.*, 1978) and consequently a plethora of experimental approaches have shown the responsibility of the N-terminal region of MyBP-C for these interactions (Whitten *et al.*, 2008; Kensler *et al.*, 2011; Lu *et al.*, 2011; Luther *et al.*, 2011; Mun *et al.*, 2011; Orlova *et* *al.*, 2011; Belknap *et al.*, 2014; Mun *et al.*, 2014; Harris *et al.*, 2016; Risi *et al.*, 2018; Inchingolo *et al.*, 2019). *In vitro* motility assays, biochemical ATP assays and single molecule imaging have revealed that MyBP-C can activate the thin filament at low [Ca^{2+}] by binding actin at a location that inhibits Tm to assume its "blocked" position (Razumova *et al.*, 2006; Saber *et al.*, 2008; Previs *et al.*, 2012; Belknap *et al.*, 2014; Mun *et al.*, 2014), while at high [Ca^{2+}], MyBP-C competes with S1 or creates a vicious load that reduces maximal sliding velocity (Craig *et al.*, 2014; Mun *et al.*, 2014; Walcott *et al.*, 2015).

The N-terminus of cMyBP-C was shown to interact with the RLC (Ratti *et al.*, 2011), proximal S2 (Ababou *et al.*, 2008) and S2 (Gruen *et al.*, 1999) of HMM and most recently the myosin mesa (Nag *et al.*, 2017). This clearly implies a role of modulating myosin but it not yet clear how and what is affected. Phosphorylation of MyBP-C reduced the interaction between myosin and MyBP-C (Gruen *et al.*, 1999; Toepfer *et al.*, 2013; Nag *et al.*, 2017) suggesting that unphosphorylated cMyBP-C inhibits myosin possibly through the IHM. PKA treatment of WT mice releases a large fraction of myosins from the thick filament, while PKA phosphorylation in MyBP-C knockout mice did not affect the fraction of myosins shifting away from the thick filament. MyBP-C knockout studies on mice showed thick filaments with less structural order than WT mice (Kensler and Harris, 2008), with a lower fraction of myosins in the IHM (Zoghbi *et al.*, 2008) and an increased force generation (Stelzer *et al.*, 2006). Furthermore, ablation of MyBP-C disrupts the SRX in mice (McNamara *et al.*, 2016), possibly by a reduced number of myosin in the IHM. This supports the notion that MyBP-C plays a role in modulating the SRX by tethering the myosin to the IHM, which is regulated by phosphorylation.

To elicit the modulating role of MyBP-C plays in muscle contraction and why it is a prolific site for mutations, a more challenging model that combines the molecular understanding with physiological observations is required (Heling *et al.*, 2020).

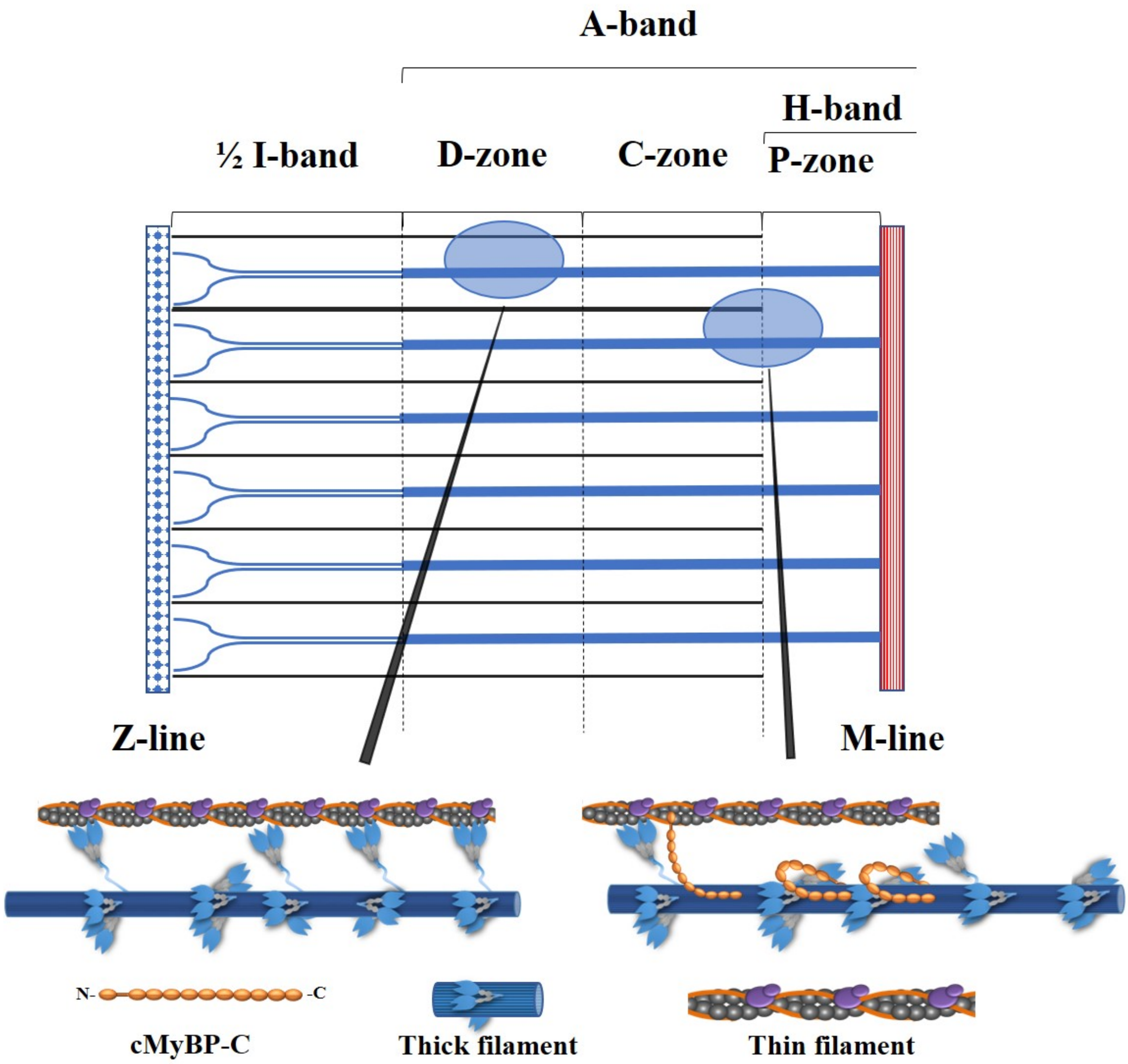

Figure 1.7 Schematic Diagram of Half Sarcomere Organisation. Model of the roles and positions of myosin binding protein C and myosin. MyBP-C is only present in the C-zones where it possibly has differential interactions between both myosin and actin. The right hand "zoom" shows a part of the C-zone and the P-zone. Note that myosin may go into the SRX without the influence of MyBP-C as is shown in the D-zone. Figure adapted from (Heling *et al.*, 2020).

1.4.2 Regulatory Light Chain

Regulatory light chain (RLC) phosphorylation and dephosphorylation has long been established to be and on/off switch for smooth muscle activity (Lowey and Trybus, 2010), releasing the myosin heads from the IHM into a state available for actin binding upon phosphorylation (Wendt *et al.*, 1999). Unphosphorylated smooth muscle myosin has a very low ATPase activity and is unable to create sliding velocity *in vitro* (Trybus *et al.*, 1997). Striated muscle myosins are not regulated by RLC phosphorylation in an on/off fashion, but RLC phosphorylation does affect the structure and function of the myosins. Phosphorylation of Ser-15 in human cardiac muscle RLC by myosin light chain kinase (MLCK) causes the myosin head to move into the interfilament space affecting the structure of myosins along the filament (Levine *et al.*, 1996). This is supported by MLCK treatment of tarantula thick filaments, showing a disruption of myosin heads in relaxed conditions (Craig *et al.*, 1987; Padrón *et al.*, 1991). MLCK phosphorylated recombinant RLC in permeabilised rat muscle increased the maximum power and velocity compared to dephosphorylated or non-phosphorylatable RLC, showing a 4-fold increase (Scruggs *et al.*, 2009; Toepfer *et al.*, 2013), while polarised fluorescence revealed that the equilibrium between open and folded states of myosin shifted more towards the DRX state of myosin upon RLC phosphorylation (Kampourakis and Irving, 2015). This suggest that unphosphorylated RLC regulates the SRX and that phosphorylation moves the myosins from the SRX into the DRX (Levine *et al.*, 1996; Colson *et al.*, 2010).

The role of RLC phosphorylation in heart failure remains unclear. Hearts from HCM patients showed an increase of phosphorylated RLC compared to donor hearts (Toepfer *et al.*, 2013), even though HCM mutations on the RLC domain inhibit the possibility to be phosphorylated (Szczesna *et al.*, 2001). Studies with two human β-cardiac myosin constructs which contained the S1 and either a short (2-hep HMM, no prox. S2) or long (25-hep HMM, with prox. S2) section of S2 showed that under RLC phosphorylation the ATPase activity was similar with a k_{cat} of ~2.5, but that dephosphorylated RLC caused a 40% decrease of ATPase activity for 25-hep HMM, an effect not seen in 2-hep HMM. This showed that prox. S2 interacted with S1 to go into the SRX upon phosphorylation of the RLC (Nag *et al.*, 2017).

1.4.3 Temperature

Increases in temperature were shown to induce a greater proportion of myosin heads to go into the SRX in skeletal muscle, which extends the lifetime of ATP turnover. Whether this SRX relation with temperature is also present in cardiac muscle is not clear, but this may provide a new method to preserve transplantation hearts. Donor hearts have a limited lifetime of ~4 h due to the risk of rigor mortis as a result of ATP depletion (Stringham *et al.*, 1992). Donor hearts stored at higher temperatures may increase the organ shelf life by forcing more myosin into the SRX which would increase the time to rigor mortis by reducing the metabolic rate. The problem with this approach is that the activity of other enzymes is increased at high temperatures, leading to a higher metabolic rate. It would be more beneficial to develop a strategy to force myosin into the SRX at lower temperatures.

1.5 Physiological Importance of the SRX

The average human body consumes approximately 8 MJ/day in modern society, which can be broken down into several components. Most energy is consumed by basic cellular functions essential for life, like homeostasis, cell division and protein synthesis. This is collectively known as the basal metabolic rate (BMR). Another large part of energy is used in a process called adaptive thermogenesis, which responses to environmental changes, like temperature exposure or nutritional ingestion. The third component of energy use is physical activity. Any intake of energy not utilised during the day is stored in fat, glycogen or proteins (Zurlo *et al.*, 1990; Stewart *et al.*, 2010).

Obesity is a worldwide issue, and a major risk factor for chronic diseases like coronary heart disease, Type 2 Diabetes Mellitus and cancer. According to the WHO (World Health Organisation, 2018), in 2016 nearly 2 billion adults were overweight, 25% of which were classified as obese.

Modulating the number of myosin in the DRX or SRX may prove to be potential therapeutic solution by disrupting the IHM to increase the energy use (Cooke, 2011). Increased energy consumption in skeletal muscle with no changes in energy consumption would lead to 7 kg weight loss over a year. A treatment disrupting the IHM, and thus the SRX, combined with exercise and a diet could be a potential strategy to treat obesity (McNamara *et al.*, 2015).

As mentioned above, the SRX may offer the missing link between increased ATP usage and clinical hypercontractility seen in HCM. Indeed, high incidences of mutations occur in domains that play a pivotal role in the IHM, thought to be the underlying structural of the SRX. Some hypothesize that the role of the SRX in the heart is to reserve myosin heads for when they are needed as an economical way of saving energy (Hooijman *et al.*, 2011; Anderson *et al.*, 2018). Stretching the sarcomere leads to an increased force output, which might be the result of SRX to DRX recruitment of myosin heads (Linari *et al.*, 2015; Irving, 2017). Cardiac SRX may therefor play a role in the Frank-Starling effect (Ait-Mou *et al.*, 2016; Reconditi *et al.*, 2017)

Several small molecule drugs to control the number of myosins functionally available have been developed and are in clinical trial as treatment for heart disease. Omecantiv mecarbil binds near the nucleotide binding site and increases cardiac contractility by speeding up the release of inorganic phosphate, increasing the number of myosin S1 strongly bound to actin (Malik *et al.*, 2011).

Mavacamten inhibits cardiac contraction and decreases myosin ATPase activity possibly by positioning the S1 in a folded back IHM configuration (Anderson *et al.*, 2018).

1.6 The Dual Control of Muscle

It has long been known that there might be a thick filament-based mechanism that modulates muscle output. The complex structure of the multiprotein assembly that is the thick filament have troubled the determination the structural components and their location. Improvements in high-resolution cryo-EM techniques however have opened new avenues for generating well-defined myosin thick filament structures (Cheng, 2015; Nogales and Scheres, 2015).

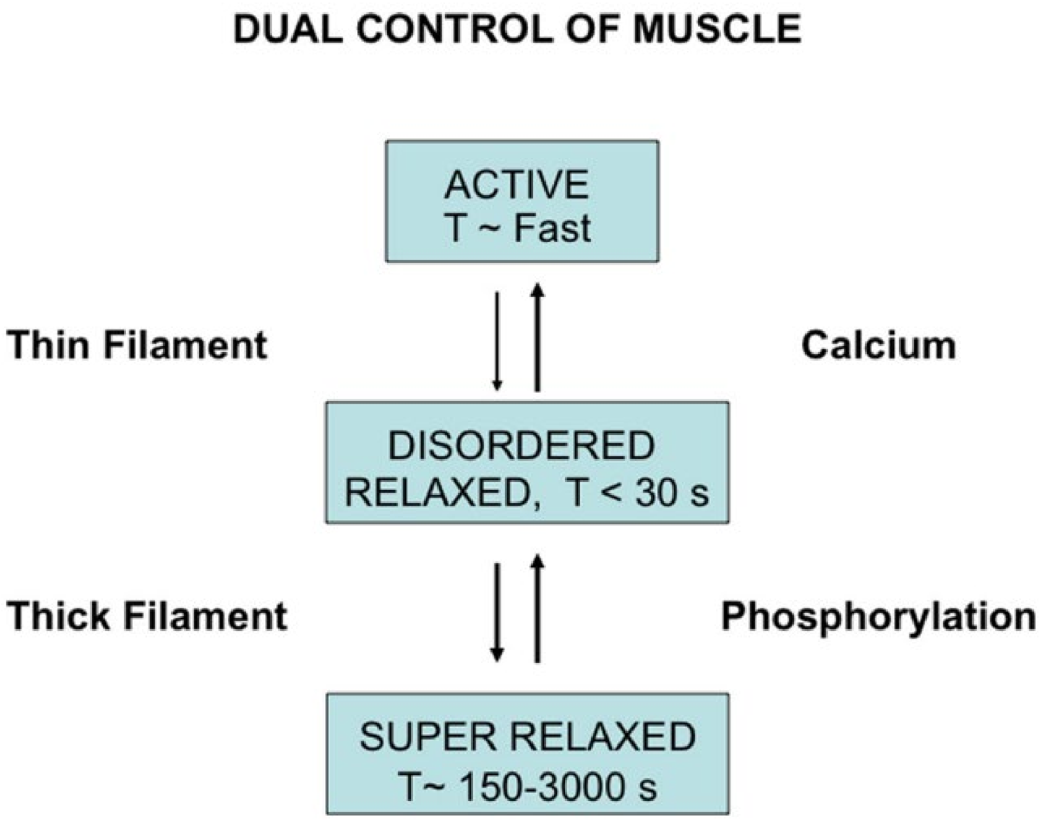

Figure 1.8 | Dual Control Model of Muscle Contraction. Three states of myosin in striated muscle. Active state has a high ATP turnover of > 1 s^{-1}. DRX has an ATP turnover rate of < 0.033 s^{-1} while the SRX exhibits strongly inhibited ATP turnover at a rate of > 0.00033 s^{-1} and < 0.0067 s^{-1}. Transfers between the states are controlled by calcium activation of the thin filament and phosphorylation of the thick filament. Figure from (McNamara *et al.*, 2015)

The discovery of the novel super relaxed state of myosin with a subsequent discovery of the highly ordered arrangement of myosin heads folded back onto the thick filament gave rise to the model shown in **figure 1.8.** MyBP-C and the RLC are strongly linked to the SRX, as are environmental influences like forced stretch and temperature. These factors suggest a physiological basis for this strongly inhibited state.

The Dual Control of Muscle model (McNamara *et al.*, 2015) states that there are three states of myosin ATP hydrolysis. The fast-active state, the disordered-relaxed state and the super-relaxed state. Activation of DRX heads is achieved via the steric blocking model of the thin filament, dependent on calcium binding. Phosphorylation of the RLC and MyBP-C enable the myosin heads to leave the SRX and join the DRX.

1.7 Aim of this Thesis

ATP hydrolysis of motor myosin in striated muscle exists in three states, active, DRX and SRX. The active state is regulated by the steric blocking model of the thin filament while the DRX and SRX are likely regulated through phosphorylation of the regulatory light chain and myosin binding protein-C. The SRX contributes to a low metabolic rate of relaxed muscle and may serve as a protection of the muscle during stress, but ablation of the SRX may lead to cardiomyopathies like HCM. HCM has been strongly linked with MyBP-C, a thick filament associated accessory protein existing in the C-zones of the A-band. Ablation of MyBP-C was shown to disrupt the SRX. This would suggest that the myosins in SRX are localized to the C-zones. However, the spatial arrangement of the SRX and DRX hydrolytic states within the sarcomere remains to be clarified.

The aim of this project is to biochemically map the ATPase activity within the sarcomere, using a combination of modern high-resolution single molecule imaging techniques and novel biochemical analysis. This can be put into broader context to understand what proteins play a role in maintaining the SRX and what implications mutations have on the presentation of HCM.

2. Experimental Methods

2.1 Buffers and Reagents

The buffers used in this study were prepared at room temperature with purified water at a resistance of 18.2 mΩ cm^{-1} from a Synergy® ultrapure water (Type 1) system.

All buffers were stored at 4°C. All reagents were of analytical grade and purchased from Sigma-Aldrich UK or Thermo Fisher Scientific UK.

Rigor buffer

50 mM imidazole, 12mM Mg-acetate, 0.5 mM EGTA, 106 mM MOPS, pH 7.0.

Fibre equilibration buffer

6 mM imidazole, 8 mM Mg-acetate, 70 mM Propionate pH 7.0, 5 mM EGTA, 7 mM ATP, 1 mM Na-azide.

Fibre skinning buffer

6 mM imidazole, 8 mM Mg-acetate, 70 mM Propionate pH 7.0, 5 mM EGTA, 7 mM ATP, 1 mM Na-azide, 0.5% (vol/vol) Triton X-100.

Fibre storage buffer

6 mM imidazole, 8 mM Mg-acetate, 70 mM Propionate pH 7.0, 5 mM EGTA, 7 mM ATP, 1 mM Na-azide, 50% (vol/vol) glycerol.

ATP solution

For imaging purposes an ATP solution was prepared off 15 nM fluorescent Rhodamine ATP (excitation: 570, emission: 590) and 150 nM unlabelled “dark” ATP. To reduce the freeze-thaw cycles and preserve the fluorophore the solution was aliquoted to 50 µL and flash-frozen before storage at -20°C.

2.2 Myofibrils

The myofibrils used in this study were from the psoas muscle of rabbit from laboratory stock. The fibres were skinned and glycerinated according to the following procedure.

2.2.1 Fibre preparation

Muscle fibres 3-4 cm in length were dissected from rabbit psoas muscle and attached to a toothpick under low tension. The fibres were equilibrated in fibre equilibration buffer near 0°C. The buffer was refreshed each half hour for 2 hours. The fibres were then chemically skinned at 4°C overnight in fibre skinning buffer. Skinning disrupts the cell membrane and removes a fraction of the ATPases and ion pumps, allowing exogenous control over ATP and [Ca^{2+}] (Wood *et al.*, 1975). After skinning the buffer was refreshed with fibre storage buffer and equilibrated at 4°C for 2 hours before storage at -20°C.

2.2.2 Sample preparation

Preparation of the sample was done around 0°C to avoid any protease activity. First, sections of muscle fibres were cut and equilibrated in rigor buffer for 1 hour. Then the fibres were cut in 1 mm or smaller cubes and homogenised (Dremer FreeWheeler Cordless Moto-Tool® Model 850 Two Speed) twice at high speed (20,000 RPM) for 10 seconds and low speed (15,000 RPM) for 5 seconds with a 30 second break in between. To check the efficacy of homogenization the sample was inspected on phase contrast light microscope. If the solution contained sufficiently dispersed single myofibrils the sample was pelleted by centrifugation at 2000 x G for 15 minutes in a cold centrifuge. The pellet was washed with fresh fibre buffer, to remove nuclei and other cell debris. This process was repeated several times.

Myofibrils are a naturally sticky substance. Therefore, before homogenization of a sample, the "drill" bit was checked under a stereoscopic microscope for any dried myofibrils. Myofibril residues affect the efficacy of the homogenizer and potentially contaminate the sample. Myofibril residues were removed using tweezers and a scalpel blade and all the mechanical parts of the homogeniser were serially washed with 70% ethanol and dH_2O.

Another method to filter the fragments that did not break to single myofibrils was the use of a filter membrane. However, attempts to clean the sample up more have only resulted in the total loss of all fragments. Longer homogenization times did lead to shorter single myofibrils with higher levels of cell debris.

The sample was stored on ice or in the fridge until used, within 48 hours.

2.3 Optical Setup

2.3.1 Flow chamber

A microfluidic flow chamber was used for all experiments in this thesis. A standard microscope slide (Thermo Fisher Scientific) was cleaned with pure ethanol and purified water (18 mΩ cm^{-1}). Two holes (ø 3 mm) were created with electric hand drill with a diamond coated dental drill tip (Dremel). Double-sided tape was cut with a printer (Explore Air, Cricut) to form 10mm x 15mm gasket. Cleaned (as above) coverslips (24 mm x 40 mm; #1.5 thickness) were coated by adding 5 µL of 15µg/mL Poly-L-Lysine to the cover slip and using another clean coverslip to drag the solution across the surface. The cover slips were set to air dry for 30 minutes. The top surface of the double-sided sticky tape was removed to produce a 180 µm thick adhesive and the coverslip, coated side down, was placed on top to create the enclosed flow chamber **(figure 2.1)**

Before introducing the myofibrils, the flow chamber was filled with rigor buffer for 30 minutes, followed by 30 µL of the sample solution. This step increased the diffusion of the myofibrils across the flow chamber instead of accumulating at the entrance of the flow chamber. The sample was left to incubate for 30 minutes at room temperature before flowing

60 μL rigor buffer through the flow chamber to wash away any fragments and myofibrils that did not adhere to the coverslip. Finally, 10 μL of the ATP solution was flowed through.

2.3.2 Single molecule fluorescent microscopy

Experimental measurements were acquired using a custom build oblique angle fluorescence (OAF) microscope build on an Olympus IX50 inverted microscope frame (Wang et al., 2017). In OAF microscopy the illumination beam is highly inclined which increases the intensity of the fluorescence 2.8 fold and reduces the background intensity 3.1-3.5 fold, enabling clear images of fluorescently labelled single molecules when compared to epifluorescence (Tokunaga *et al.*, 2008). Rhodamine ATP was excited using a 561 nm diode OBIS LS laser (Coherent, USA) at 5 mW focussed through a 100x objective. Imaging was performed using time lapsed illumination. The synchronicity between the laser and camera was controlled by an Arduino. Laser ON times were fixed at 100 ms while the laser OFF times varied between 100 ms to 4900 ms to have frame interval times ranging between 200 ms and 5 s. The total acquisition period for all experiments was 5 minutes. Images were acquired using the OrcaFlash 4.2 camera (Hamamatsu, pixel size 63.2 nm) using 1x1 binning.

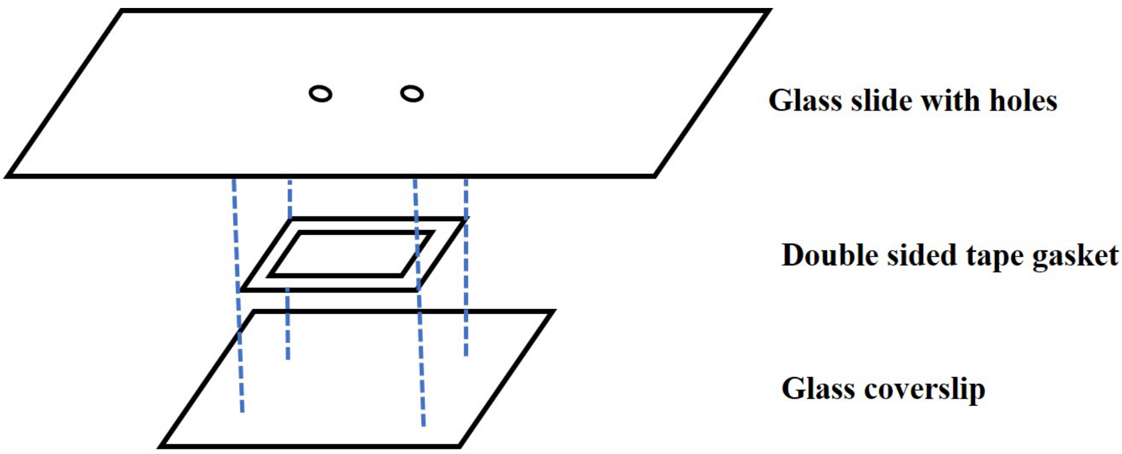

Figure 2.1 | Flow chamber construct. Microfluidic flow chamber. The holes drilled in the glass slide allow for solutions to be introduced. Figure adapted from (Springall *et al.*, 2016)

2.3.3 Stochastic Optical Reconstruction Microscopy (STORM) imaging

The non-invasive nature of light in conventional fluorescence microscopy allows the imaging of biological specimens with little agitation. This technique enables the observation of dynamic processes as the occur in molecular and cell biology. The development of a multitude of fluorescent tags, like green fluorescent protein (GFP), enabled to specifically label biological components. Multi-colour fluorescent microscopes therefore were able to follow multiple components in real time in live cells. However, the relatively low spatial resolution of optical light microscopes leaves many subcellular structures too small to discern. Molecular complexes and subcellular components often exist in the nanometre-micrometre scale length, while the structural features when observed with light become blurred or difficult to resolve at ~0.2 µm. Other techniques like electron microscopy (EM) have a much higher resolution but this does not obtain the possibility to observe the dynamic processes in live cells with the label specificity. In the last decade to bridge the gap between light microscopy´s specificity and EMs resolution several new techniques were developed collectively referred to as super-resolution imaging techniques. One such technique is STochastic Optical Recontstruction Microscopy (STORM) (Bates *et al.*, 2013).

In light microscopy, a point source of light like a fluorophore, appears as a spot larger than the source of light. The intensity profile of that spot follows a Gaussian distribution. In order to distinguish the source of light as a single object, the must follow a criterium which mathematically determines the distance between two objects before they become indistinguishable. Multiple fluorophores in close proximity cannot be localised. With STORM imaging the obstacle is overcome by using optically switchable fluorophores. These molecules can be switched between and fluorescent and non-fluorescent states. By activating a small subset of fluorophores per image cycle, before activating a stochastically different subset of fluorophores, this ensures no overlap in fluorophores. Consequently, this allows for the localisation of the fluorophore in high resolution. After a sufficient number of cycles, a high-resolution image can be constructed from the measured locations of the fluorophores **(Figure 2.2)**. This is the basis of STORM image reconstruction.

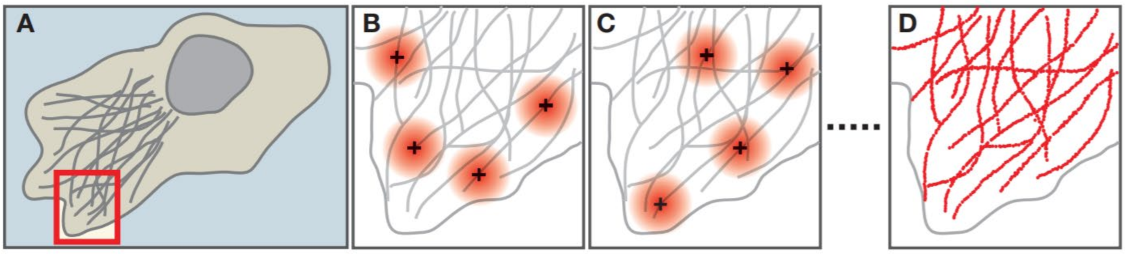

Figure 2.2 | STORM imaging procedure. Schematic representation of the procedure of STORM imaging. **(A)** Schematic of a cell in which the region of interest, in this case the grey filaments, are labelled with fluorophores. **(B)** A limited set of fluorophores (black plus sign) is activated so that their images (large red circles) recorded by the microscope do not overlap. Their positions are resolved by fitting for the centre of the spot. **(C)** A stochastically different set of fluorophores are activated, and their locations are determined as before. **(D)** After sufficient cycles of activating fluorophores and localising their positions, a high-resolution image can be reconstructed by plotting the measured positions of the positions of the fluorophores (red dots). Image taken from (Bates *et al.*, 2013).

3. Data analysis

Myosin in relaxed muscle exists in two subpopulations, the DRX and the SRX, with ATP turnover rate constants that differ at least 5-fold (Hooijman *et al.*, 2011). Because these hydrolytic states have only been measured using bulk kinetics, the spatial location of these subpopulations at the sarcomere level remains unclear. In experiments at the single molecule level, a stochastic event is often observed, which would not have been identified in an measurement of the ensemble (Li and Xie, 2011). Using single molecule imaging to study transcription factors *in vivo* provided a direct way to characterise the kinetics of the dynamic interactions with other components like DNA (Gebhardt *et al.*, 2013). Furthermore, it was clear that single molecule studies can determine the spatiotemporal qualities of these processes. We used single molecule studies to elucidate the spatiotemporal arrangement of ATP hydrolysis states in relaxed sarcomeres.

To do this we studied the single turnover kinetics of the myofibrillar ATPase. **Figure 3.1a** shows single fluorescent ATP molecules binding to a single myofibril immobilised in a microfluidic flow chamber as described in 2.3.1 under relaxing conditions (no Ca^{2+}).

Photobleaching of fluorophores and dissociation lead to the loss of signal. How these factors influence the duration of binding events is unattainable under continuous laser exposure, due to the fast photobleaching of fluorescent protein. To overcome this factor time lapse images were recorded, with a fixed laser exposure time and a varying laser off time described in section 2.3.2. This allowed us to track fluorophores over a long period of time, extracting the dissociation rate constant k_{off} and photobleaching rate constant k_{pb}.

The different time lapse intervals were set at 200 ms, 500 ms, 1 s, 2 s, 3 s and 5s for a period of 5 minutes. Images were taken at room temperature.

A myofibril generally consisted of 16-20 sarcomeres, where the sarcomeres were 2.3 µm (± 0.09 µm SEM, n=3 flow chambers) in length which corresponds to sarcomere lengths in relaxed conditions (Knight and Trinick, 1982).

The observed fluorescence was located mainly in bright bands perpendicular to the myofibril. The length of the bright bands was 1.5 µm (± 0.06 µm SEM, n=3 flow chambers) which resembles the width of the sarcomeric A-band, which contains myosin. Close inspection of the middle of the A-band suggest a slight reduction of fluorescence (**figure 3.1b**), which may correlate with the position of the M-line. We conclude that the majority of Rhodamine ATP molecules selectively bind myosin.

3.1 Data Subtraction

To investigate the single turnover kinetics, we needed to perform rigorous image analysis.

The duration and trajectory of single molecule ATP molecules emitting a fluorescent signal were tracked using the FIJI/ImageJ (Schindelin *et al.*, 2012) plugin TrackMate (Tinevez *et al.*, 2017).

To improve the detection of molecules by Trackmate, the images were cropped and straightened to individual myofibrils with little to no background (**figure 3.1b**). This also helped with the comparison between myofibrils later on.

Videos >1000 frames created performance issues with TrackMate, only recognizing a subfraction of all spots that were spotted by eye. To improve this, videos were subdivided to 500 frame videos, which reduced the gap of binding events recognised by eye and by the software.

We considered ATP bound to myosin if the molecule was localized for at least two consecutive frames. Molecules that seemed localised for a single frame were neglected to avoid including unbound molecules in the calculations.

3.2 STORM

The fluorescent emission from the fluorophores terminates from ON to OFF through two processes (explained in more detail in **section 3.6**). This loss of emission can be used to reconstruct the structural representation of the sample in super resolution (Bates *et al.*, 2013). **Figure 3.1c** shows the super resolution image of the myofibril, made with Microsoft Excel using the extracted X and Y coordinates of the ATP binding events. Note the clear representation of the A-bands. Close inspection of these bands indicates the presence of two sub bands, with a slight gap in the middle, where the M-line would be.

3.3 Occurrence and Average Lifetimes of ATP binding events

To determine the occurrence of binding events spatially, we calculated and plotted a histogram of the number of tracks in horizontal space using a 25 nm bin which is shown by the black line in **figure 3.1d**

Since the SRX inhibits ATP hydrolysis resulting in longer ATP turnover lifetimes, the measured lifetimes of the fluorophores residing on the myofibril should be prolonged in regions where myosin is in the SRX state. The average lifetimes in those regions should therefore be longer, while the occurrence of events is lower. The spatial arrangement of the average lifetimes was obtained using a custom written Visual Basic script within Microsoft Excel. Taking in consideration the bin size and occurrence of events, as well as the lifetime of each event it calculated the cumulative lifetime of the tracks within that bin. The average lifetime within each bin was easily attained by dividing the cumulative lifetimes by the occurrence which was plotted as a histogram (blue line) in **figure 3.1e**. **Figure 3.1f** shows the occurrence and average lifetime plotted on the same graph. The peaks of the average lifetimes globally align to the same location as the peaks of the occurrence along the myofibril, namely the A-band.

3.4 Superposing Sarcomeres

From the data on the myofibrillar level it is hard to determine how the occurrence and the lifetimes align within the sarcomere let alone the different zones within the A-band. The lifetime and occurrence data were therefore further improved by superposing the sarcomeres along the myofibril using Microsoft Excel.

By eye it was estimated where the Z-lines were located, judged by the dark patches along the myofibril. The XY coordinates of the events within that sarcomere as well as the lifetime attached were extracted **(figure 3.1g)**. To superimpose the different sarcomeres, the X-coordinates of the first sarcomere were corrected to 0 and a histogram of the occurrence of events was plot shown as the black line **Figure 3.1h**. The following sarcomere (red line in **figure 3.1i**) was fitted against this first set using the sum of squared differences (SSD), with the SSD value closest to 0 determining the best fit. These two sets of data, as well as subsequent data was used to create a cumulative occurrence histogram **(figure 3.1j)** that represented multiple sarcomeres in the myofibril.

Since the lifetime data was attached, the average lifetimes could be determined as described above. The histograms of the occurrence and the lifetimes plot were plot at the level of the sarcomere **(Figure 3.1k)**.

Within the A-band there is a certain degree of repetition of high, low, lowest, low, high occurrence of events. The lowest occurrence seemed to be most localized to the centre of the A-band, which suggests that this could be the M-line. This point was considered to be 0 on the x-axis and **figure 3.1l** shows the histograms plot to this new axis, with the y-axis cutting through the middle of the sarcomere.

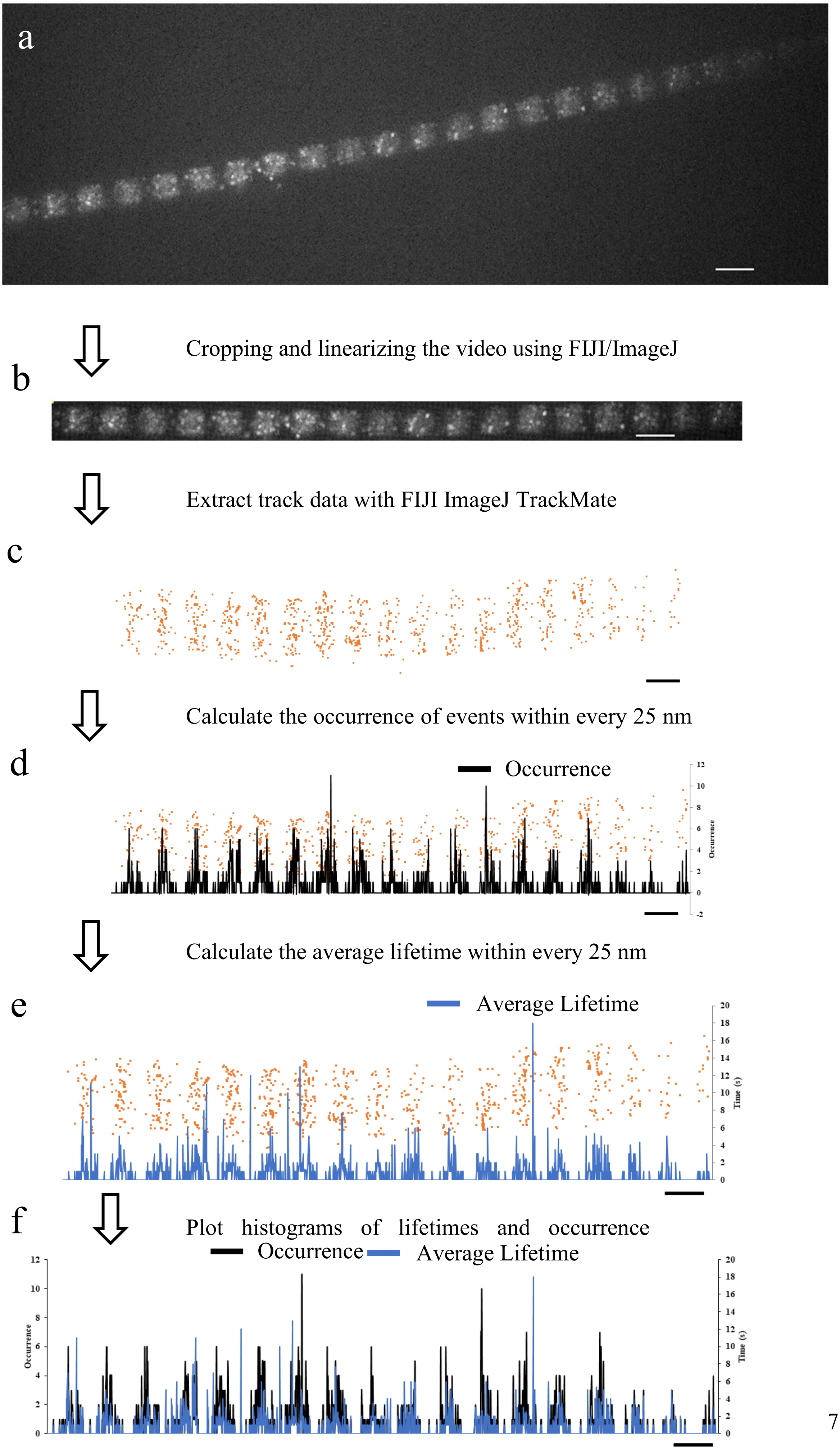

a
b
Cropping and linearizing the video using FIJI/ImageJ
Extract track data with FIJI ImageJ TrackMate
c
Calculate the occurrence of events within every 25 nm
d
Occurrence
Calculate the average lifetime within every 25 nm
e
Average Lifetime
Time (s)
f
Plot histograms of lifetimes and occurrence
Occurrence
Average Lifetime
Occurrence
Time (s)

Plot histograms of lifetimes and occurrence together

g

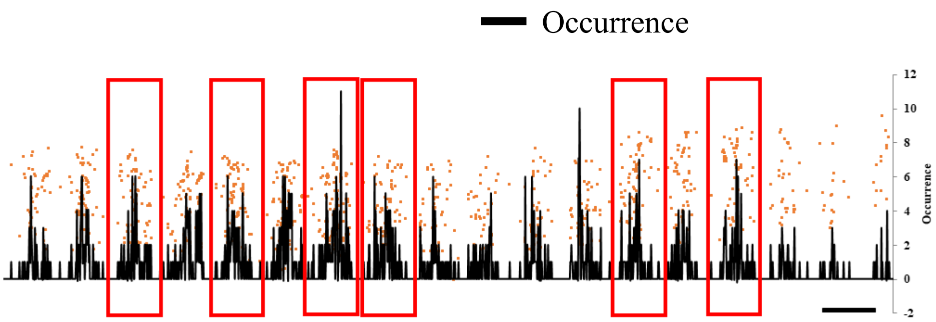

Superpose sarcomeres of myofibrils using the sum of squared differences

h

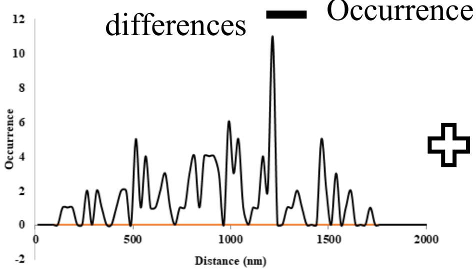

i

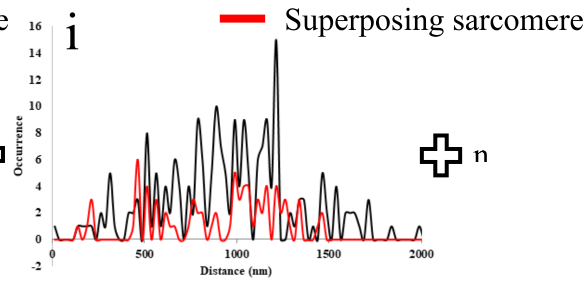

j

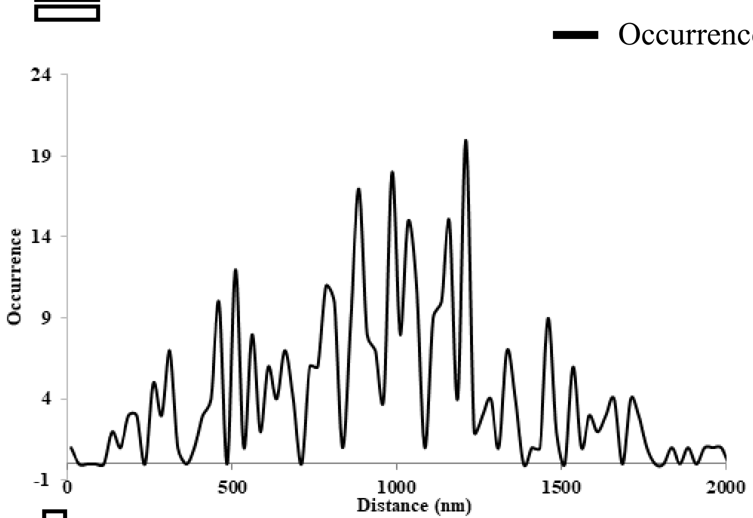

Plot the average lifetime histogram

k

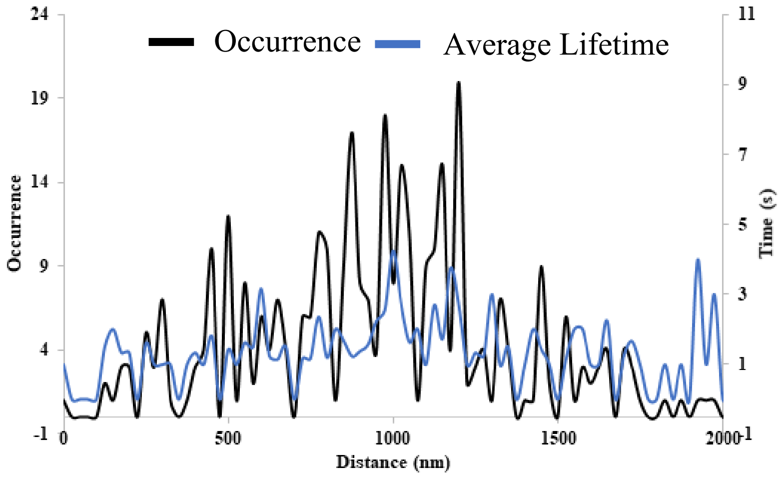

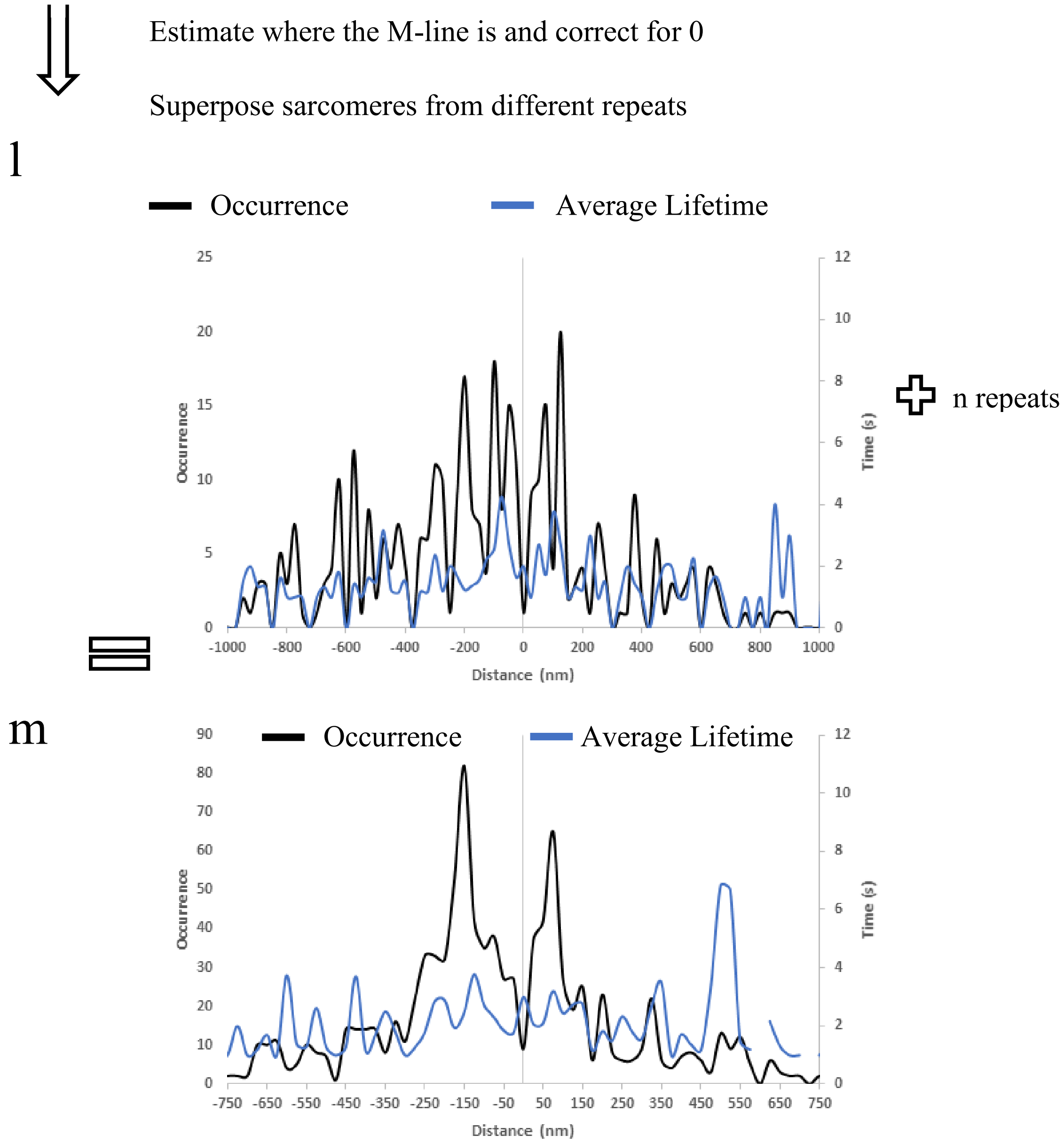

Figure 3.1 | Visual workflow of the data analysis. (a) Actual image of a single rabbit psoas myofibril with 15nm Rhodamine ATP. The brighter bands are ~1.5 µm wide, approximating the length of the A-band. This video was recorded with 1 second total frame interval. **(b)** The video cropped and straightened with FIJI/ImageJ to show only the myofibril, ready for data extraction using TrackMate. **(c)** 2D STORM image using the x and y coordinates of the tracked molecules. **(d)** Histogram showing the occurrence of events within every 25 nm (blue) on the same STORM image **(e)** STORM image from **c** with a histogram of the average lifetimes (blue line) every 25 nm **(f)** Overlaid histograms of the average lifetimes and the occurrence across the myofibril **(g)** Identification and subtraction of single sarcomeres (in the red boxes) along the myofibril **(h)** Histogram of occurrence of the first sarcomere corrected to 0. **(i)** Following alignment, the occurrence of events was collected to create a cumulative occurrence histogram. Subsequent sarcomeres (red line) were aligned to this histogram using the sum of squared differences. **(j)** Cumulative occurrence histogram of the superposed sarcomere. **(k)** Overlaid histograms of the average lifetime (blue line) and cumulative occurrence (black line) of the superposed sarcomere. **(l)** Superposed sarcomere, with the estimated M-line corrected to 0. **(m)** Superposed sarcomere of all repeats (n=3) with 1 second time-lapse time. The scale bar in **a-g** is 2.5 µm, the width of the plots in **h-l** is 2 µm and **m** is 1.5 µm.

3.6 Characterization of the dissociation rate constants

A Poisson distributed process is defined by random events happening independent of each other, with a constant rate. The fluorescent ON state, i.e. the emitting signal of the fluorophore can switch to OFF through either of two processes that follow such distributions; photobleaching rate constant (k_1) or dissociation rate constants (k_{off}) **(Figure 3.2)**, where the nucleotide is hydrolysed by the myosin ATPase.

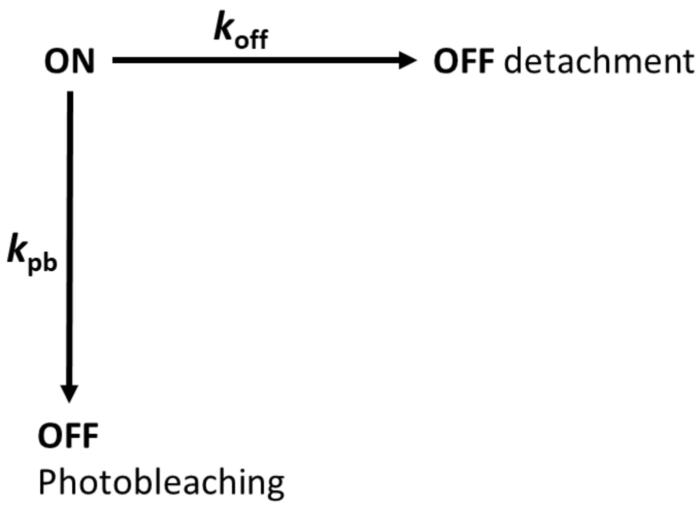

Figure 3.2 | Visual representation of the two fates of a fluorophore with the corresponding rate constants.

A Poisson distribution can be described by an exponential fit. Equation (3.1) describes a fit by an exponential decay of the occurrence of fluorophores with one effective rate constant:

$$f(t) = A \times e^{(-k_{\mathrm{eff}} \times t)} \qquad (3.1)$$

where $k_{eff} = k_1 + k_{off}$ as described by **figure 3.2**, A is the amplitude and t is the frame time. The photobleaching rate constant is subject to the intensity of the laser which is dependent on the time laser is emitting (τ_{on}) and the total time-lapse time (τ_{tl}). After all samples with a

200ms frame rate have 500 ms/s of laser exposure, while 500 ms frame rates have 200 ms/s laser exposure.

$$k_1 = k_{\mathrm{pb}} \frac{\tau_{\mathrm{on}}}{\tau_{\mathrm{tl}}} \tag{3.2}$$

So $k_{\mathrm{eff}} = k_1 + k_{\mathrm{off}} = k_{\mathrm{pb}}\tau_{\mathrm{on}}/\tau_{\mathrm{tl}} + k_{\mathrm{off}}$. Equation (3.1) and equation (3.2) can be rewritten to create a final exponential decay function:

$$f(t) = A \times e^{\left(-\left(k_{\mathrm{pb}}\frac{\tau_{\mathrm{on}}}{\tau_{\mathrm{tl}}} + k_{\mathrm{off}}\right)t\right)} \tag{3.3}$$

We utilised the scheme laid out above to determine the effective rate constant k_{eff} of Rhodamine ATP.

Effective off rate constant traces of Rhodamine ATP did not fit well to a single exponential, as can be observed in **figure 3.3a**. The linear extrapolation of the single exponential fit, by taking the log of the y axis **(figure 3.3b)**, deviated from the data, meaning a higher order exponential was involved. Indeed, a double exponential fits the data better, as shown in **figure 3.3c**, thus two exponentials were used to fit the data. Two exponential fits are consistent with our assumption that there are two populations of ATP turnover in relaxed muscle.

k_{eff} of the distribution of lifetimes across multiple time-lapse conditions were obtained by fitting equation (3.1) in Microsoft Excel using the sum of squared differences and the built in Solver function. Described above is that k_{eff} is a two-state system consisting of the photobleaching rate constant k_{pb} and the dissociation rate constant k_{off}. **Figure 3.4** shows the extracted rate constants plotted as a function of the interval times, which yields a straight line of best fit that follows equation (3.4). The slope of the function gives the dissociation rate constant, while the photobleaching rate constant is provided by the y-intercept.

$$k_{\mathrm{eff}}(\tau_{\mathrm{tl}}) = k_{\mathrm{pb}}\tau_{\mathrm{on}} + k_{\mathrm{off}}\tau_{\mathrm{tl}} \tag{3.4}$$

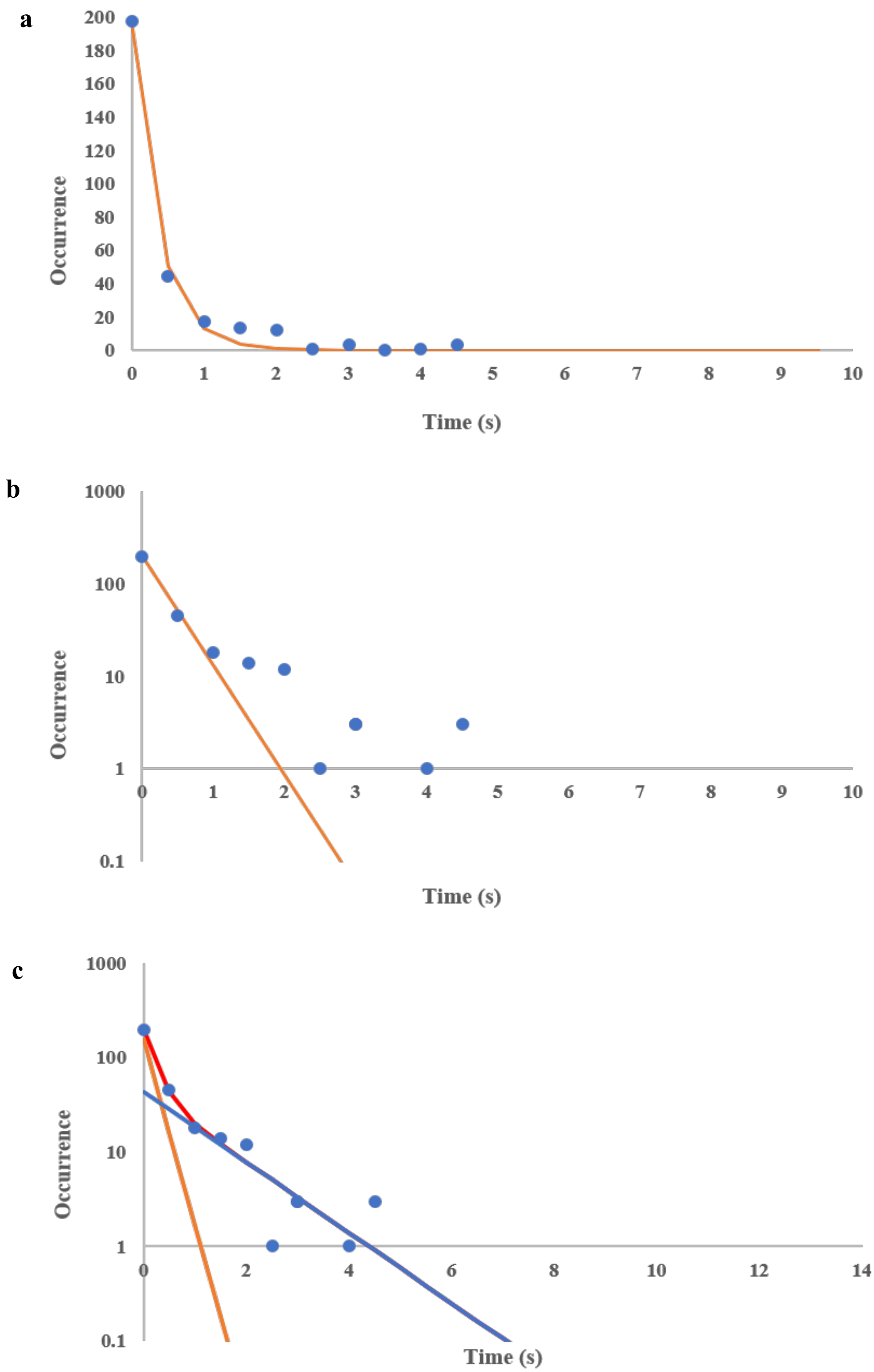

Figure 3.3 | Occurrence plotted as a function of time. **(a)** Single exponential fitting did not align well with the data, **(b)** as can be observed by linear extrapolation. **(c)** The red line is a double exponential fit that is a sum of the two single exponentials, the orange line is the fast and the blue line is the slow exponential.

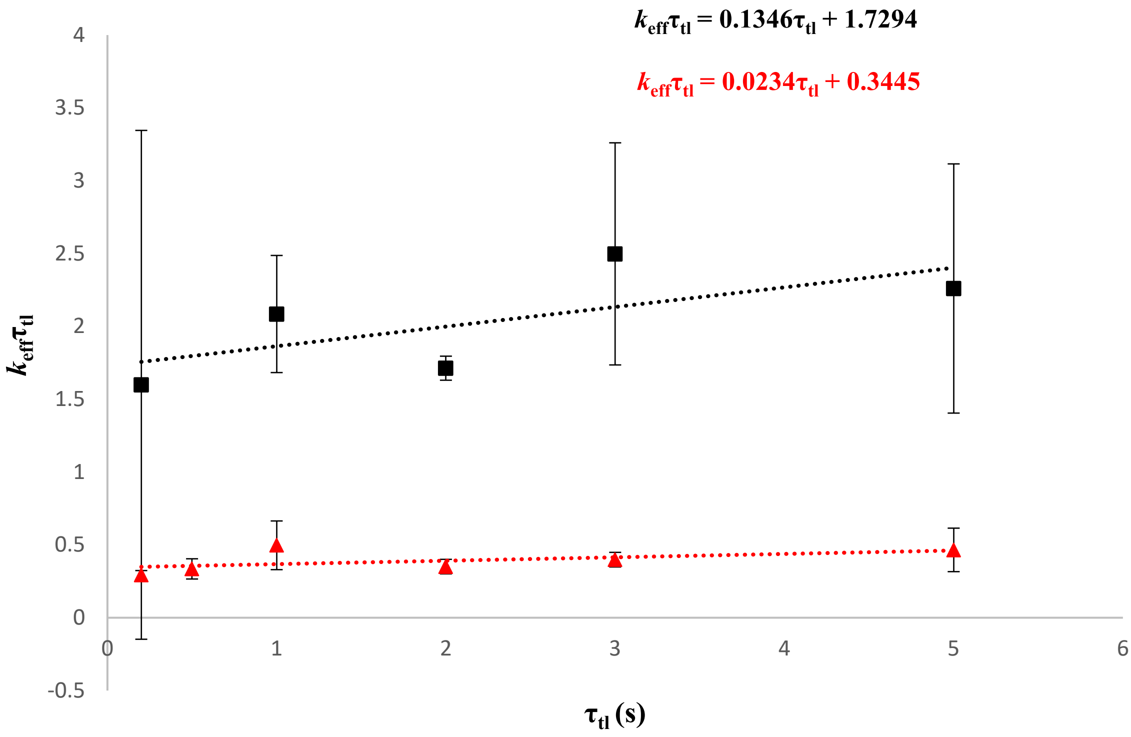

Figure 3.4 | Extracted rate constants as a function of the time-lapse time. Extracted rate constants from single and double exponentials at different time-lapse times, from 200 ms – 5 s. Line of best fit drawn by Excel. Error bars, SEM

4. Results

4.1 The Sub-Populations of ATP Lifetimes

Plotting the occurrence as a function of the average lifetime, shows the exponential distribution of the ATP binding events. With the two subpopulations yielding a fast and a slow rate of ATP turnover, as was identified to exists in muscle myosin under relaxing conditions, the occurrence of events would reflect that with a higher occurrence of short ATP lifetimes and a lower occurrence of longer ATP lifetimes.

To determine if we can identify this in our measurements, we plotted the occurrence of single binding events versus the average lifetimes at every time lapse condition (**figure 4.1**). Indeed, two distinct sub populations of ATP turnover can be observed. The red boxes show the fast turnover events while the dark blue boxes discern the slow events. The green dashed lines in figure **4.1a** represent what an exponential decay for both the subpopulations could look like, although exact calculations for this decay were not performed due to time limitations.

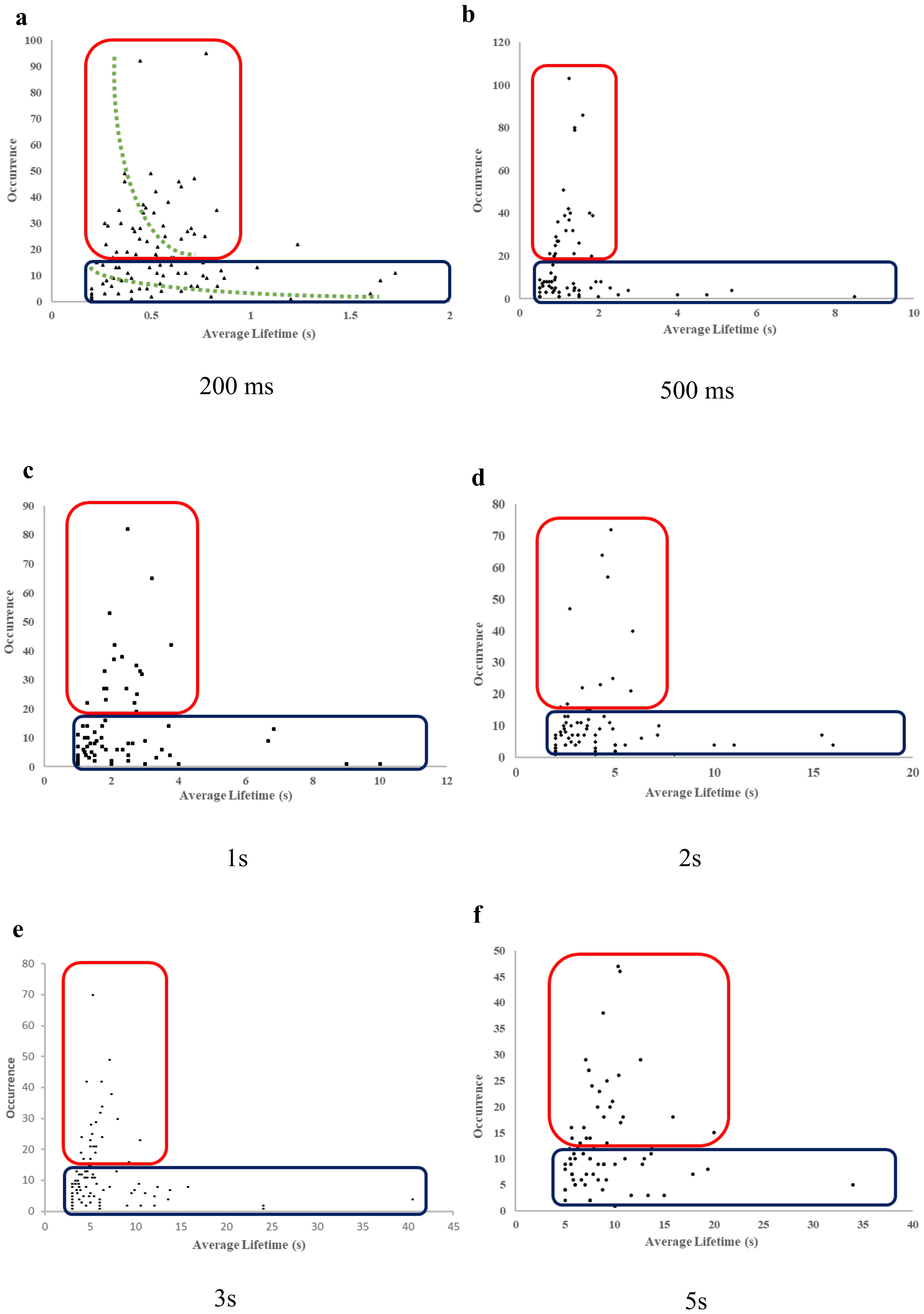

Figure 4.1 | Occurrence of binding events as functions of the average lifetime. Each plot (**a-f**) represents the cumulative occurrence of events of three repeats at each time lapse condition. Fast turnover events are captured in the red box, with the slow events in the dark blue boxes. **(a)** Green dotted line represents predicted exponential decay fit.

4.2 Spatially Resolved Arrangement of ATP Lifetimes in the Sarcomere

We hypothesized to see similarly two populations when spatially resolving for the average lifetimes and occurrence. More interesting would it be if the spatial arrangement would align with known structural properties of the sarcomere like the C-zone which is located 200-500 nm from the M-line. MyBP-C, localised to the C-zone, has been strongly linked with the SRX.

To this end we created STORM reconstructions of the superposed sarcomeres and plotted histograms for the occurrence and average lifetime at different time lapse conditions shown in **figure 4.2 a, c, e, g, i, k**. The absence of myosin nucleotide binding sites in the M-line means that no fluorescence is expected. We can observe from our STORM reconstructions that the A-band has a small region in the middle where fewer binding events were recorded. Using this we modelled the A-band regions, indicated by the blue dashed boxes.

Figure 4.2b, d, f, h, j and l show the histograms of the occurrence and average lifetimes along the superposed sarcomeres. The horizontal axis represents the distance in nanometres. The M-line, the middle of the sarcomere, is considered 0 on this axis.

The average lifetimes and the occurrence do not peak at the same special locations, something we would expect if there are two distinct populations of lifetimes within the sarcomere. Furthermore, in regions where we would expect the C-zone to be, the lifetimes are generally longer and the occurrence lower than what we can observe in the H-zone and D-zone. This is especially apparent in **figure 4.2j**. The region spanning from -200nm to 0 to 200nm represents the H-band. No actin is present here, and only a few myosin motor domains. The occurrence of binding events in that region surpasses 130. In the adjacent region that is 300 nm long, supposedly the C-zone, the occurrence drops while the average lifetime increases, a trend that inverts again more than 500 nm away from the M-line when entering the D-zone. which would suggest that MyBP-C indeed plays a part in regulating the ATP turnover.

a

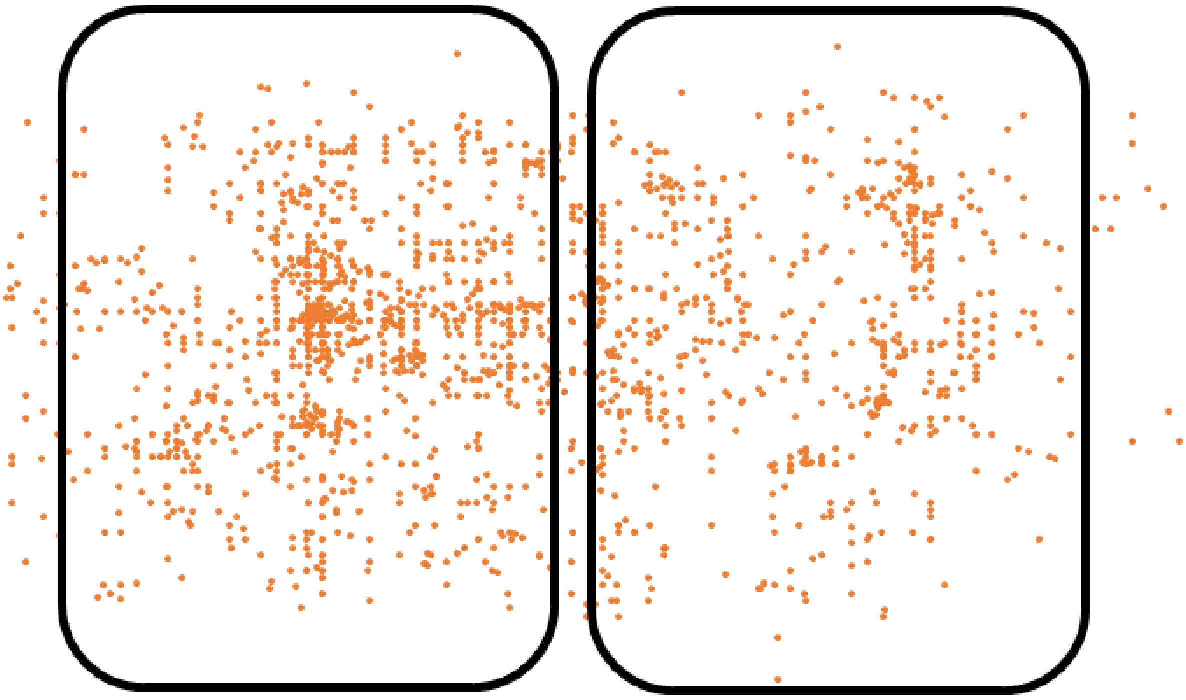

b

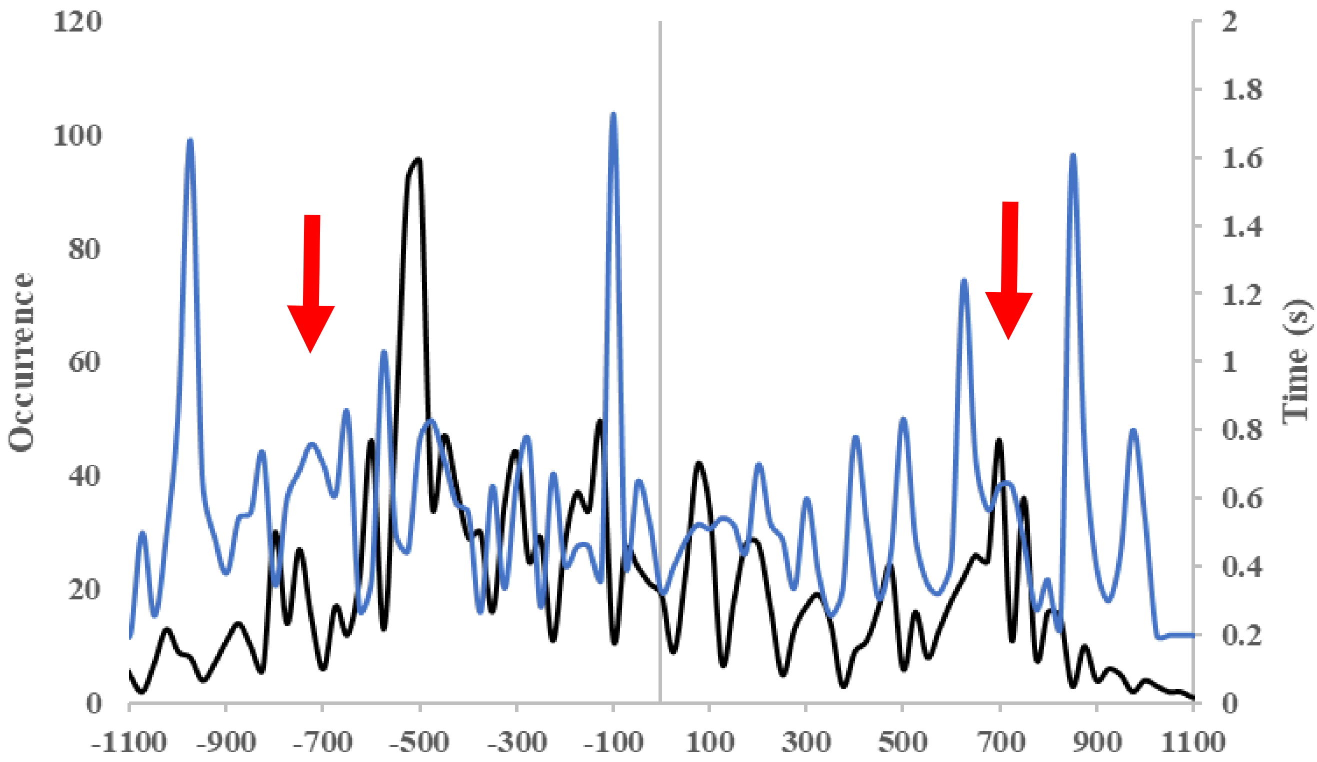

c

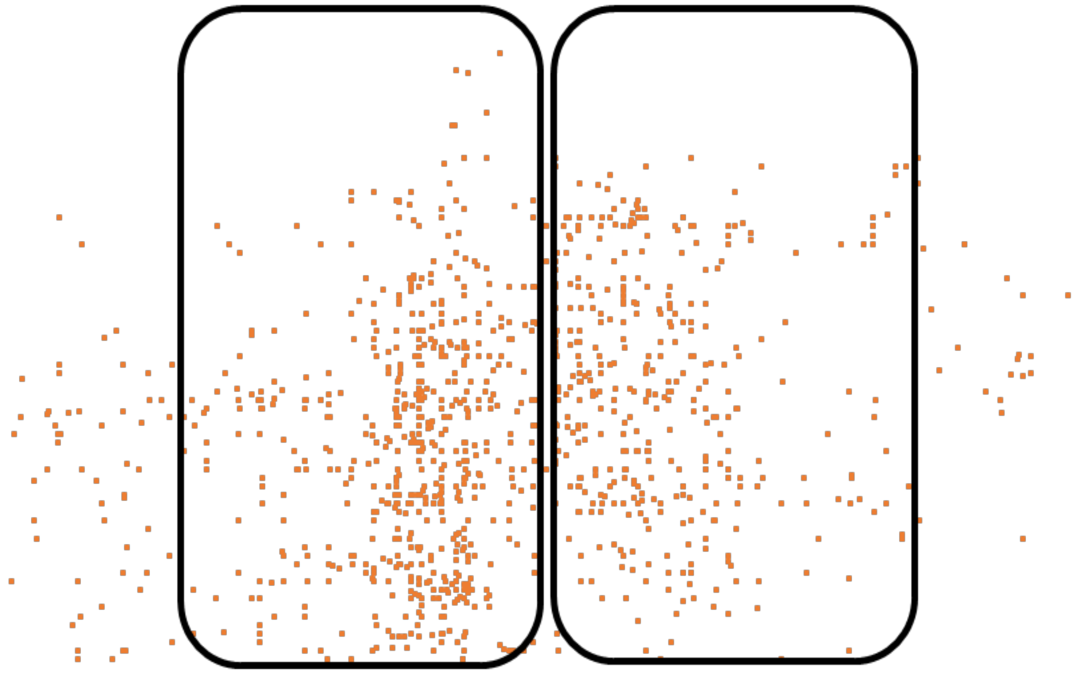

d

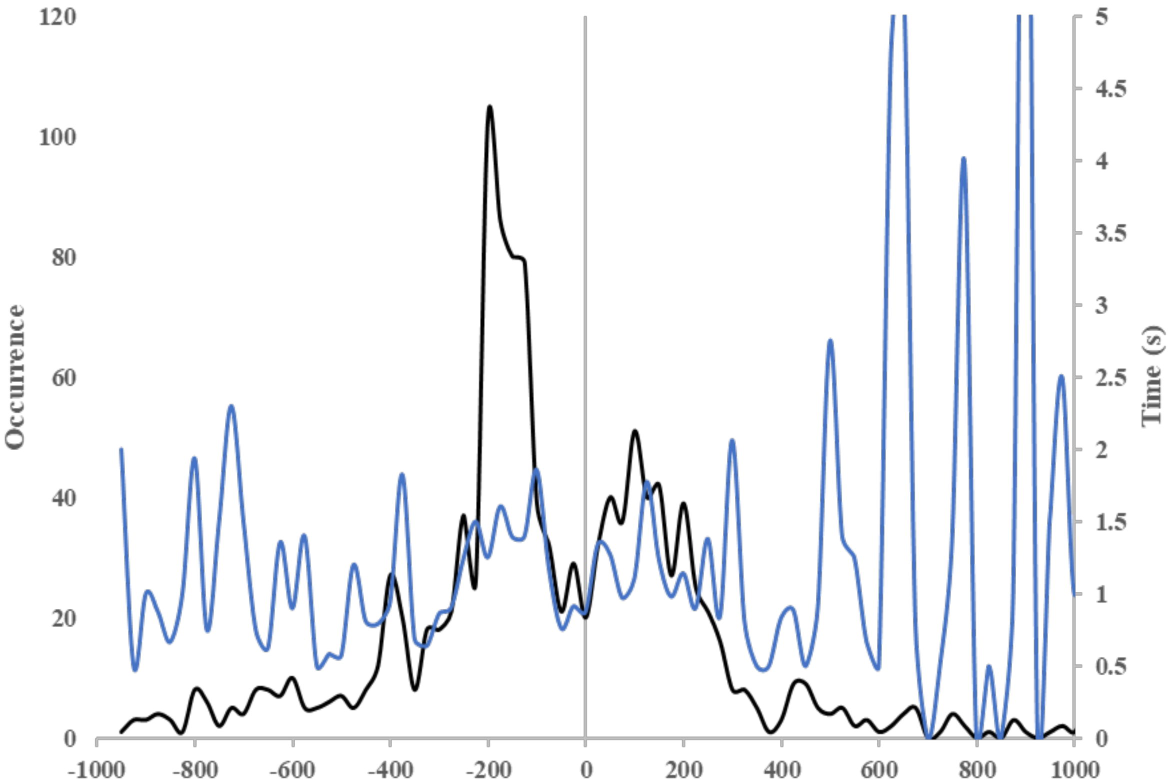

Occurrence
Time (s)
120
100
80
60
40
20
0
5
4.5
4
3.5
3
2.5
2
1.5
1
0.5
0
-1000
-800
-600
-400
-200
0
200
400
600
800
1000

e

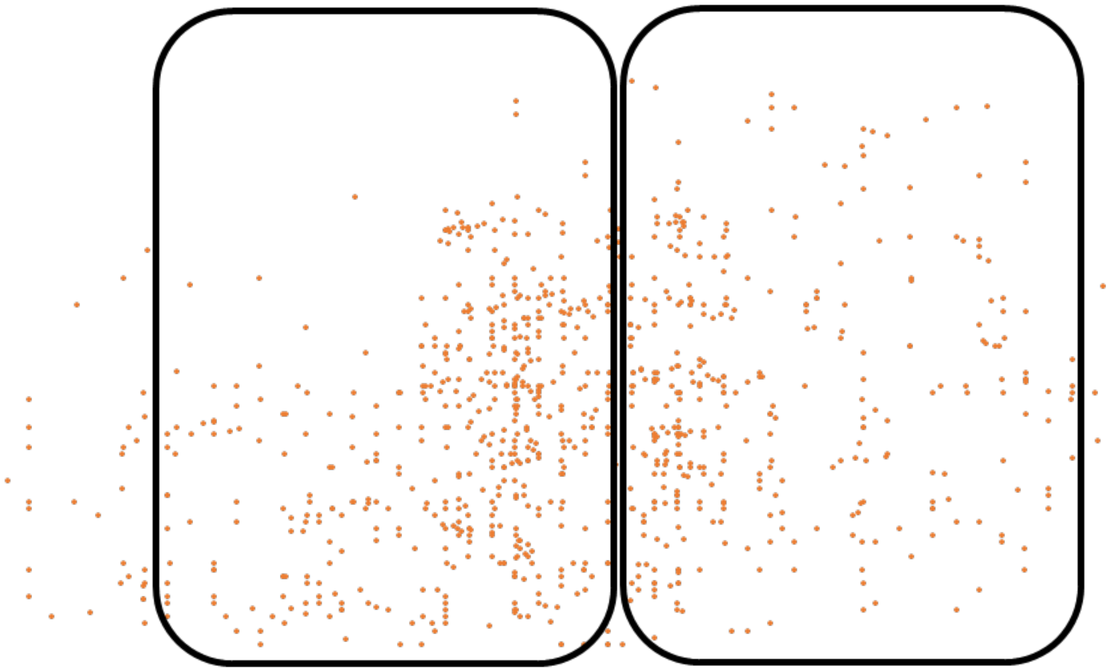

f

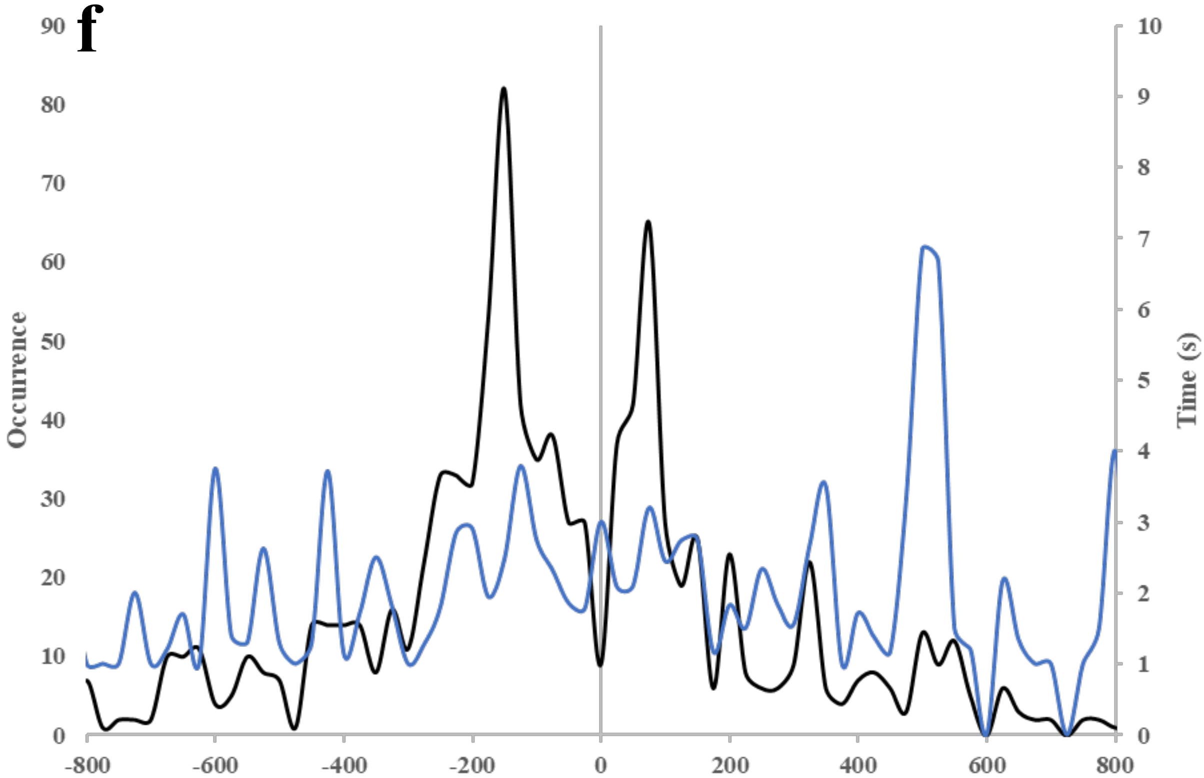
Occurrence
Time (s)
90
80
70
60
50
40
30
20
10
0
10
9
8
7
6
5
4
3
2
1
0
-800
-600
-400
-200
0
200
400
600
800

g

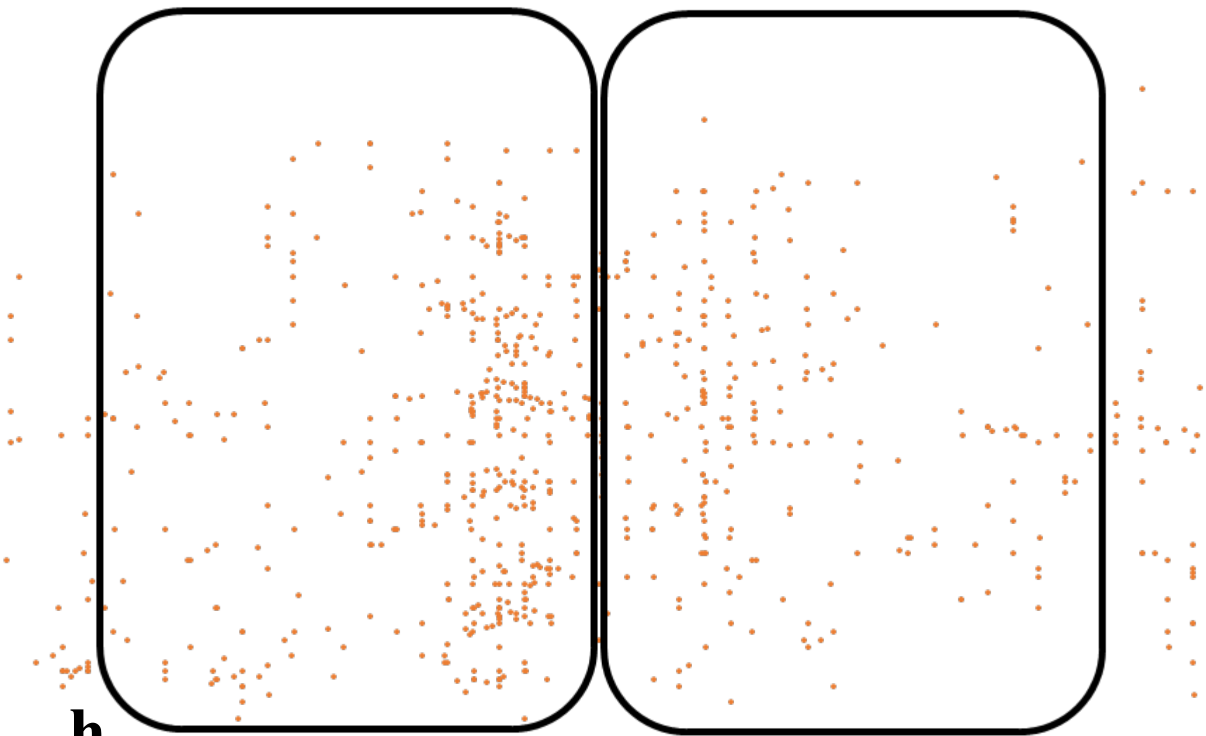

h

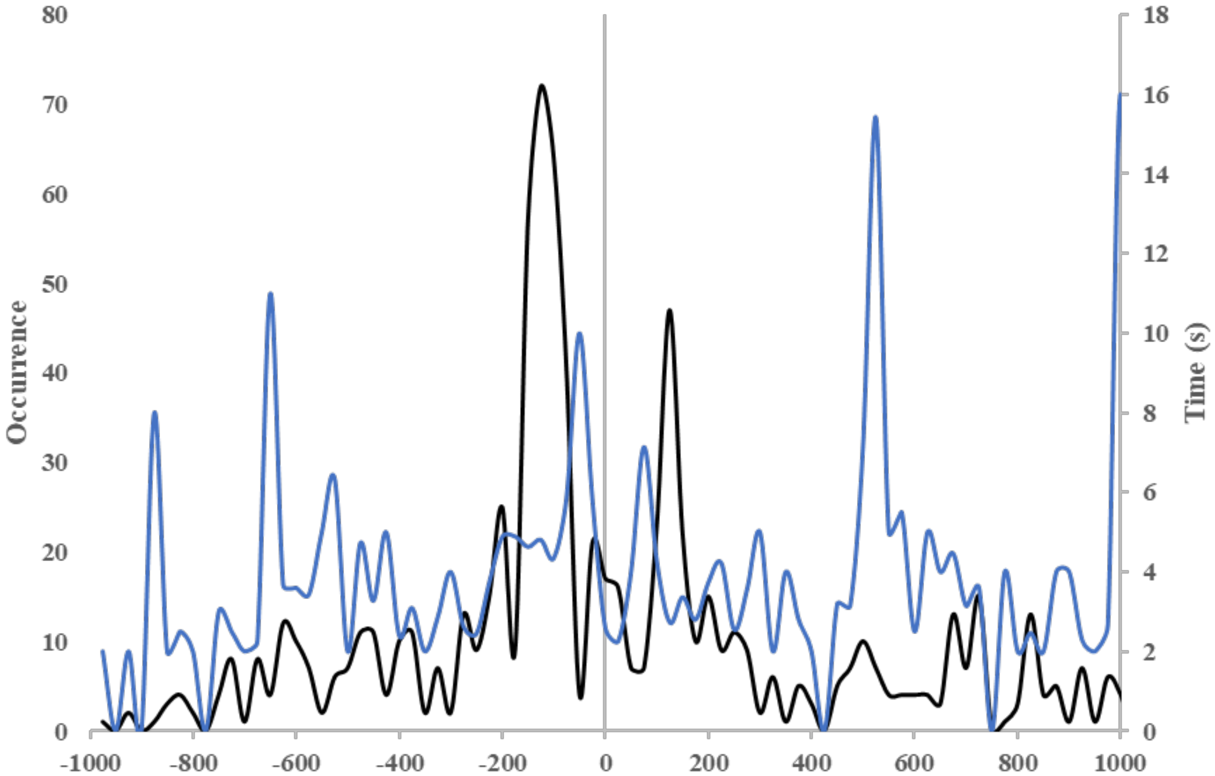

Occurrence
Time (s)
80
70
60
50
40
30
20
10
0
18
16
14
12
10
8
6
4
2
0
-1000
-800
-600
-400
-200
0
200
400
600
800
1000

i

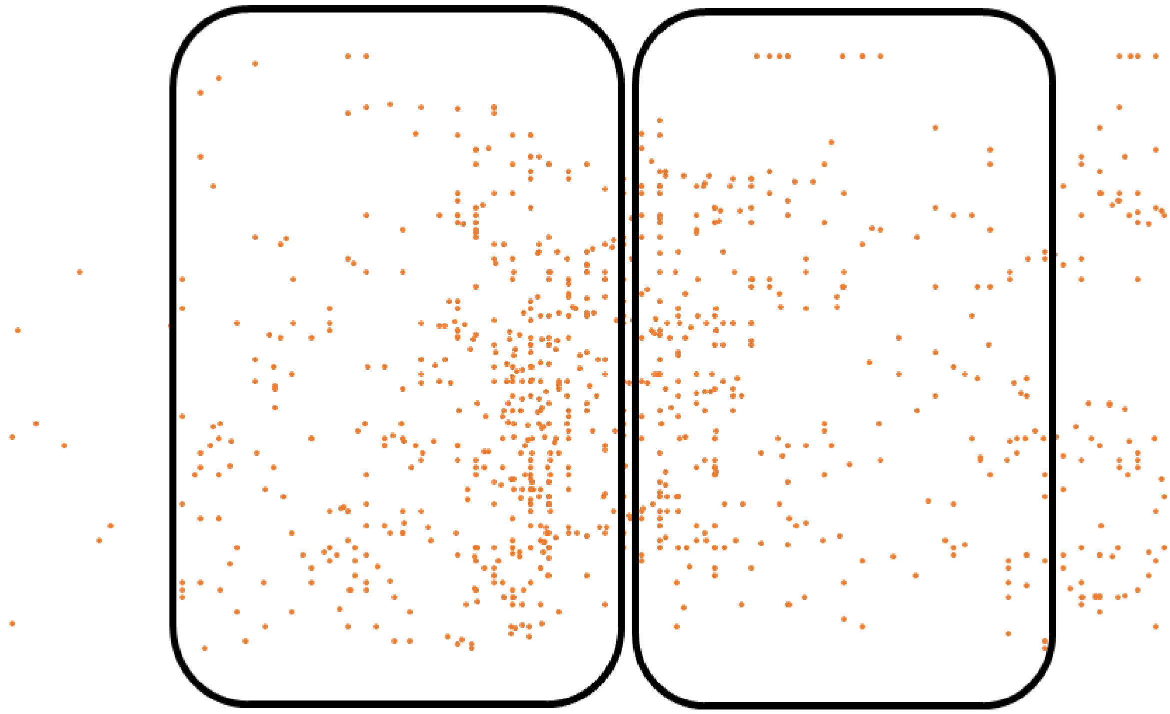

j

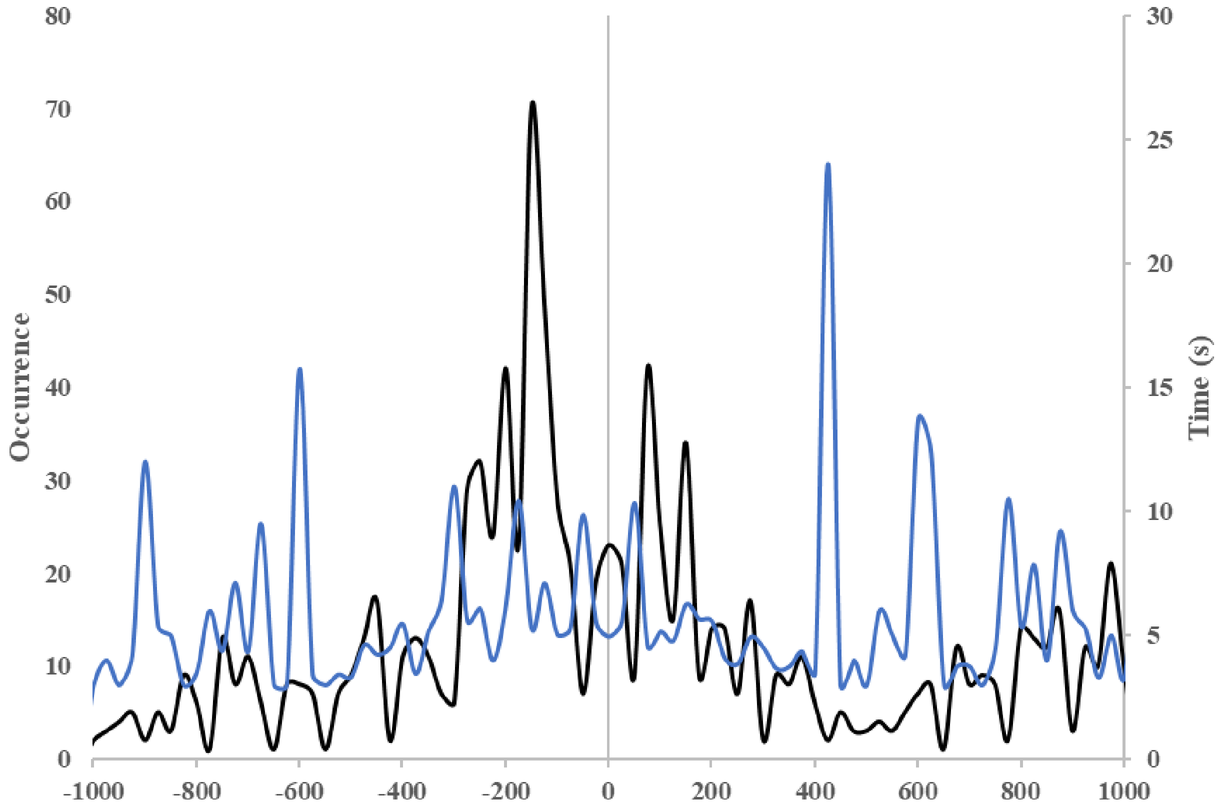
Occurrence
Time (s)
80
70
60
50
40
30
20
10
0
30
25
20
15
10
5
0
-1000
-800
-600
-400
-200
0
200
400
600
800
1000

k

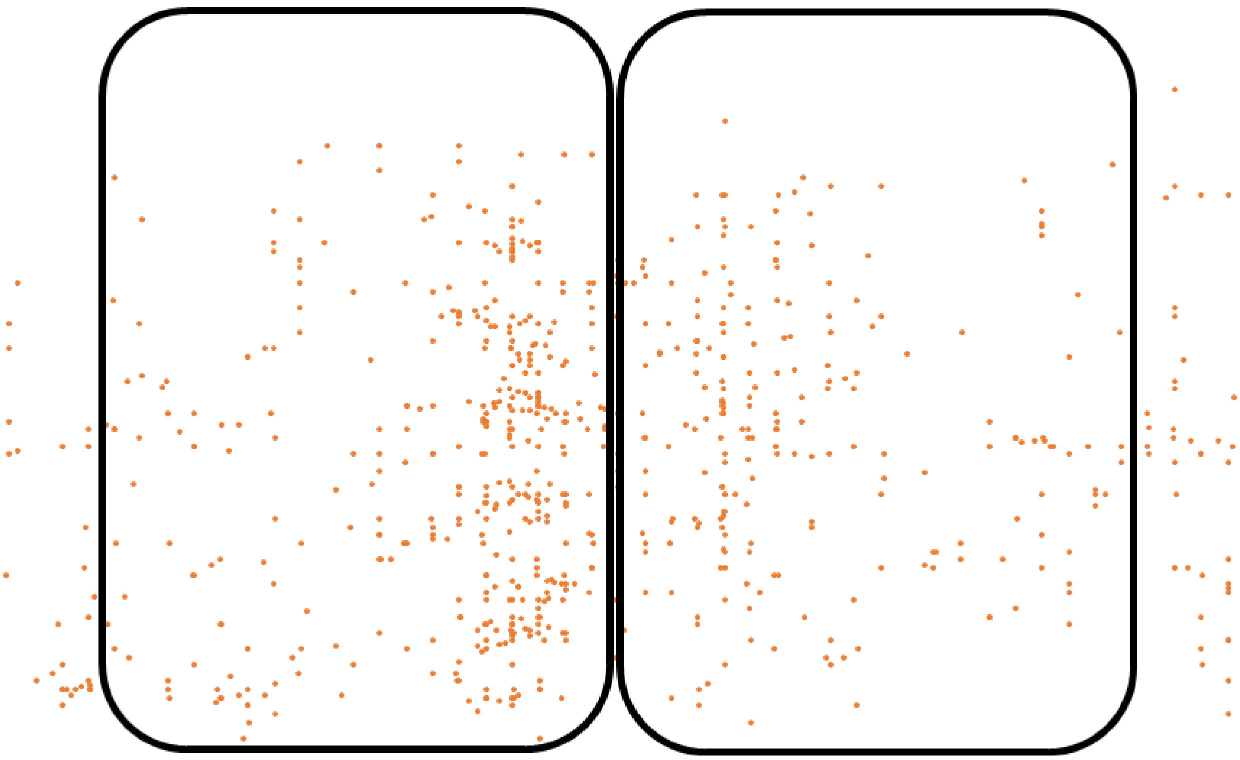

l

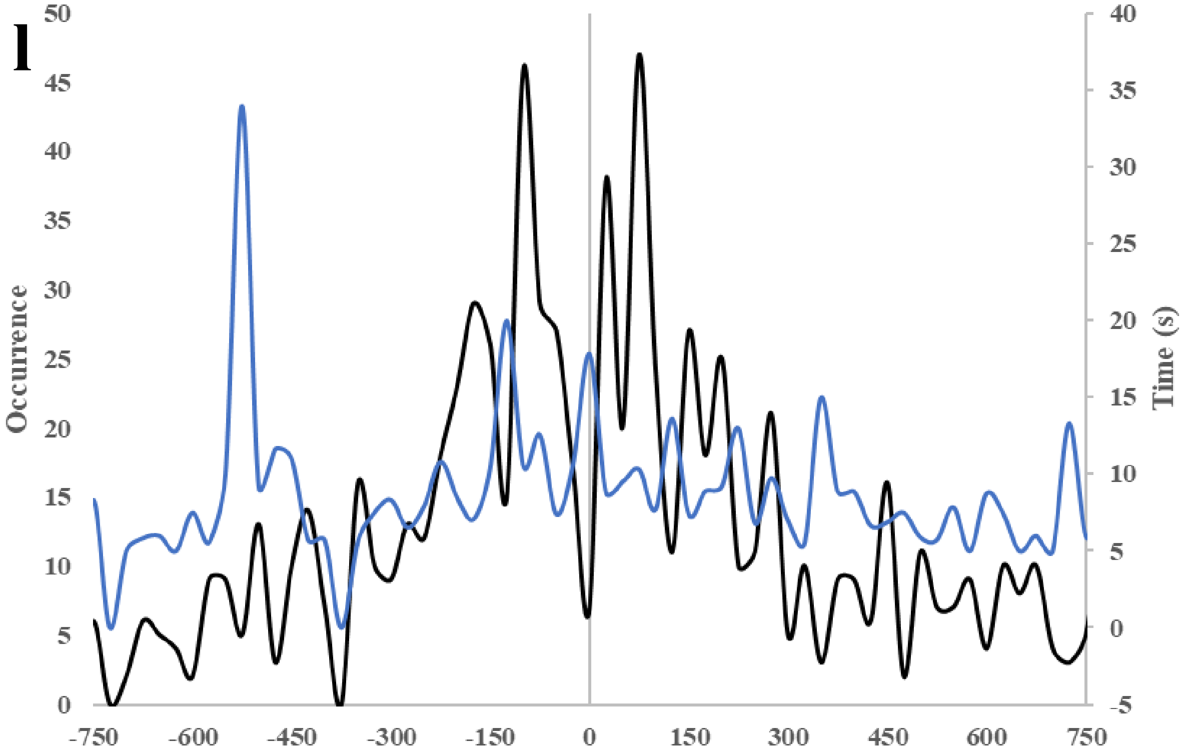
Occurrence
Time (s)
50
45
40
35
30
25
20
15
10
5
0
40
35
30
25
20
15
10
5
0
-5
-750
-600
-450
-300
-150
0
150
300
450
600
750

Figure 4.2 | Spatiotemporal map of the sarcomere. dSTORM reconstruction and the superimposed occurrence and lifetime histograms for the sarcomere at each time lapse condition. Data from 3 experimental repeats. **(a, c, e. g, i, k)** dSTORM reconstruction of all the binding events in a sarcomere. The boxes represent the A-bands, **(b, d, f, h, j, l)** shows the superimposed occurrence and average lifetimes histograms. The M-line is 0 on the x-axis. **(b)** The red arrows represent where we expect the lateral boundaries of the A-band to be.

4.3 Dissociation Kinetics

Superposing the sarcomeres allowed for the calculation of k_{off} using equation (3.4). We were able to do this for the whole sarcomere, just the A-band and half the A-band estimated from the M-line

Figure 4.3 shows the rate constants as a function of the time lapse times for the first and second exponential fit for the global sarcomere (from Z-line to Z-line). The lines of best fit, drawn by Microsoft Excel, follow equation **(3.4)** giving the ATP turnover rate constant k_{off} by the slope and the k_{pb} as the y-intercept (Gebhardt *et al.*, 2013). k_1 has a short ATP turnover lifetime of 7.4 s which is comparable to previously reported ATP turnover time of 6s in relaxed rabbit skeletal muscle (Myburgh *et al.*, 1995).

k_2 is nearly 6-fold longer at 42.7 s. The photobleaching rates are 1.7294 s^{-1} and 0.3445 s^{-1} respectively.

The 6-fold difference between these global rates are similar to the earlier reported difference between the DRX and SRX in rabbit cardiac muscle (Hooijman *et al.*, 2011), but the respective turnover rates are faster at ~7 seconds versus the previously seen ~15s in the DRX and ~42s versus ~150-200s in SRX.

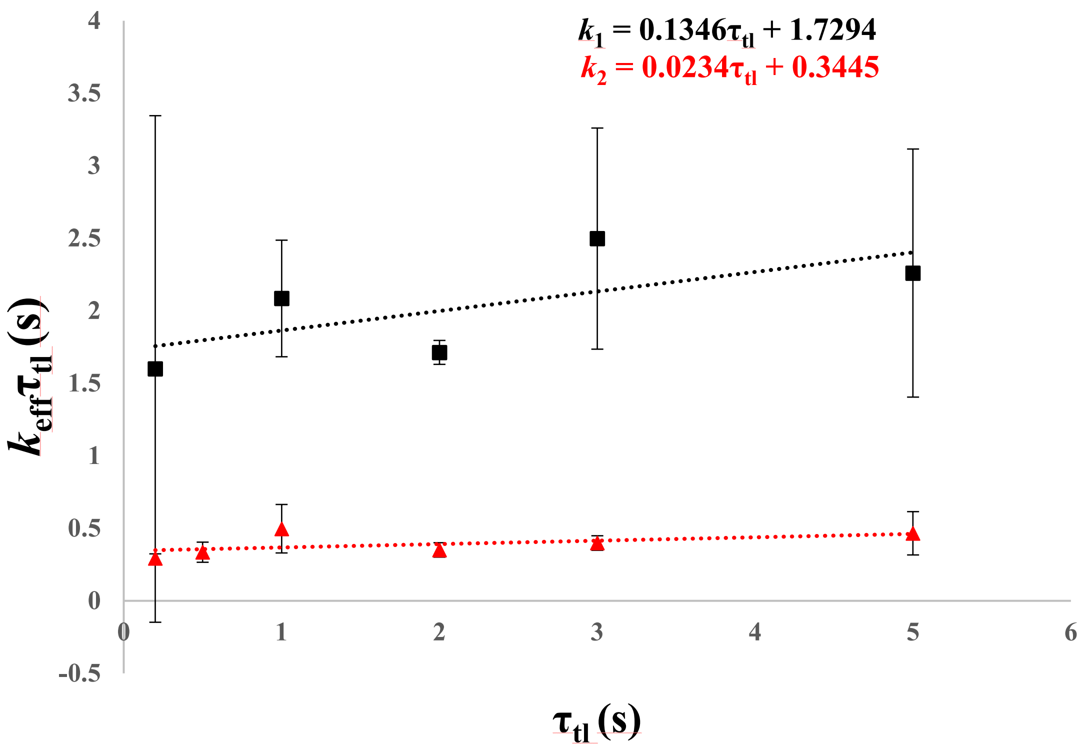

Figure 4.3 | Two ATP turnover rates by myosin in the whole sarcomere. Effective rate constants plotted as a function of the time lapse conditions. Lines of best fit are drawn by Microsoft Excel and follow equation (3.4). The conditions are 200 ms, 500 ms, 1 s, 2 s, 3s and 5s. The slow rate k_2 shown as red triangles is 5.8-fold slower than k_1 shown as black squares. The 500 ms time lapse condition of k_1 is shown but was not included to improve the fit. Data is average of 3 repeats and error is SEM.

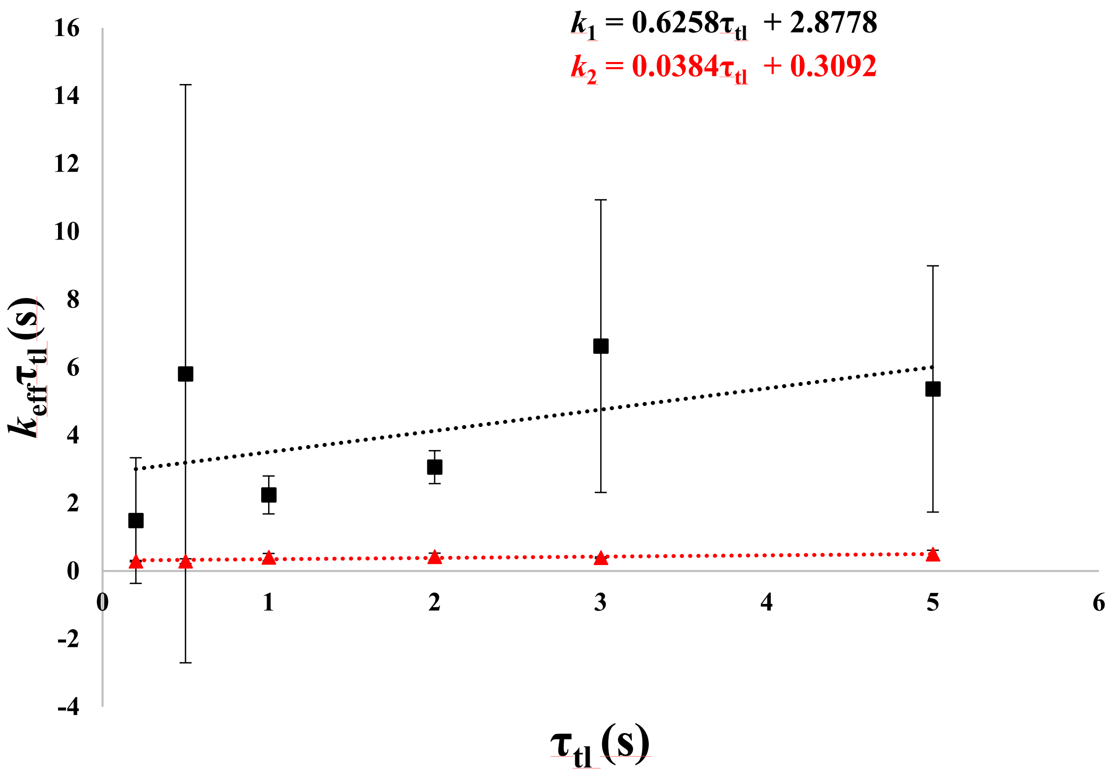

Figure 4.4 | Two ATP turnover rates by myosin in the A-band. Effective rate constants plotted as a function of times for two exponentials yields the following two lines of best fit drawn by Excel. Effective rates of fast k_1 (black squares) and the slow k_2 (red triangles) are of the same experimental conditions as in **figure 4.3**. Data is from 3 experimental repeats and errors are SEM

The lateral boundaries of the A-band were estimated from the superposed sarcomeres, taking the first peak to the final peak of the occurrence histogram (see **figure 4.2b**). The effective rate of binding events within the A-band at all time lapse rate constants are shown in **figure 4.4**. The 16- fold difference between k1 and k2 is larger than for the whole sarcomere, but the individual rates are faster for both at 1.6s and 26s respectively.

The turnover rates of half the A-band are depicted in **figure 4.5.** The M-line was estimated by eye and the boundaries of the A-band was decided as mentioned above. The 33-fold difference of the dissociation rates observed in the ½ A-band is more than double the difference between the slow and fast population at the level of the A-band level due to the k_1 being twice as fast as the k_1 for the A band, while k_2 was comparable. The difference between the fast and slow populations is nearly 6-fold of the differences between the two populations seen in whole sarcomere.

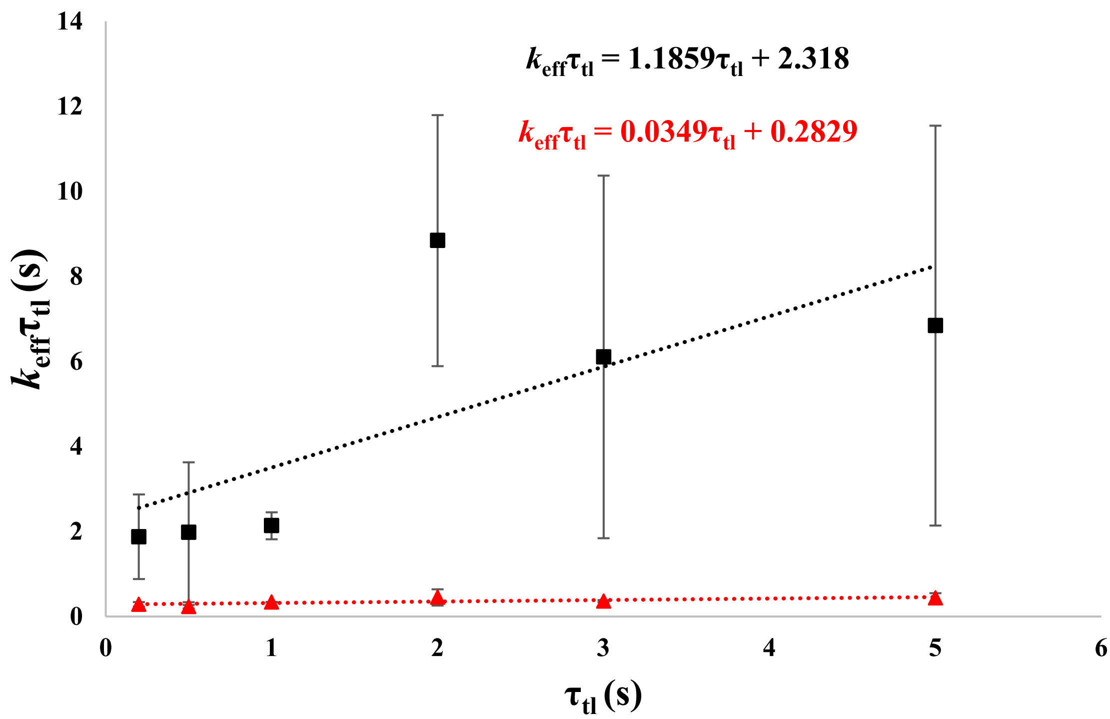

Figure 4.5 | Two ATP turnover rates by myosin in half A-band. Effective rate constants plotted as a function of times for two exponentials yields the following two lines of best fit drawn by Excel. Effective rates of fast k_1 (black squares) and the slow k_2 (red triangles) are of the same experimental conditions as in **figure 4.3**. Data is from 3 experimental repeats and errors are SEM.

5. Discussion

Bulk kinetics have shown that muscle myosin in relaxed conditions, i.e. low to no Ca^{2+} hydrolyses ATP with rate constants that fall in two distinct populations (Stewart *et al.*, 2010; Hooijman *et al.*, 2011; Naber *et al.*, 2011; McNamara *et al.*, 2015). The DRX, with myosin heads projecting into the inter-filament space, has a ATP turnover rate constant of less than 0.03 s^{-1} (Myburgh *et al.*, 1995) while the SRX has severely inhibited ATP turnover rate constants that lie closer to 0.003 s^{-1} (McNamara *et al.*, 2015). It is highly likely that the SRX is structurally linked to the sequester folded back state of myosin the IHM, but further structural studies need to completely confirm that. The spatial arrangement of the DRX and SRX within the sarcomere, if there is any, is unknown.

To determine the spatial arrangement of ATP hydrolysis states we visualised single ATP molecules binding and releasing from myosin motor domains in the sarcomere. This allowed for the study of the kinetics of this dynamic process in their native myofibrillar environment for the first time. We observed that two subpopulations of myosin exist, consistent with the literature, with distinct ATP hydrolysis rates.

The main finding of this study is that the spatial arrangement of myosin with slow ATP turnover rate constants is different to the arrangement of the faster hydrolysis state, using STORM structural reconstruction imaging. There is a discrepancy between the rates observed here and the previously reported to conclusively say we are looking at the SRX, and due to time constraints we were only able to run a minimal number of repeats leading to significant errors we believe will normalise with more experiments. Nonetheless, the methods we present in this thesis **(Chapter 3)** to extrapolate kinetic data from single molecule ATP interacting with myosin in their natural myofibrillar environment can be used for future experiments on these dynamic transient processes.

5.1 Two subpopulations of relaxed myosin

The observations of the occurrence-average lifetime plots in this study **(figure 4.1**) show that the exponential distribution of the ATP binding events can be distinguished into two populations. The superimposed histograms of the occurrence and average lifetimes show a similar relationship where the regions of higher occurrence do no coincide with the regions with slower ATP turnovers **(figure 4.3b, d, f, h, j, l)**. This suggests that the time lapse approach we used to track single ATP molecules binding to the myofibril allowed for the identification of short and long lifetimes over a variable period of time from 200 ms to multiple seconds, or even minutes is that would be desired, without the influence of photobleaching on the dissociation rate. To experiments in this study were performed with varying time lapse conditions (200ms to 5 minutes) but always for a true period of 5 minutes. This means a varying number of frames; 1500 frames for the 200ms time lapse condition while 5s time lapse conditions yielded 60 frames. This means that the exposure to the laser was significantly different between two conditions. To further elucidate the effects of photobleaching, future experiments should keep the number of frames constant so the laser exposure time between samples is the same.

5.2 Dissociation rate constants of single molecule fluorescent ATP

To test whether the subpopulations we observed have the same ATP turnover rates as the previously reported DRX and SRX, we measured the kinetics (**3.6**) of the ATPase of myofibrils per sarcomere, A-band and ½ A-band (**Figure 4.3 – 4.5**).

We found that the difference between the dissociation rates of ATP of the slow and the fast population is at least 5-fold, going as high as 28-fold. This is consistent with the the differences between the DRX and SRX in the literature which are at least 5-fold, going as high as 100-fold (Hooijman *et al.*, 2011; McNamara *et al.*, 2015).

However, the ATP hydrolysis rates we observed are considerably faster than what was suggested for the SRX (150-300 s) and DRX (~30 s) (Cooke, 2011; McNamara *et al.*, 2015), with a turnover lifetime as short as of 0.8 s for the fast population which is comparable to the rate of actin activated ATPase. This high rate was not the result of actin activated ATPase however – after all, muscle shortening was not observed, and no calcium was present to regulate the movement of tropomyosin.

The observed differences between our measured data and the literature could be the result of several factors. The muscle fibres used for all experiments were skinned and glycerinated in 2016. The quality of the muscle fibre is dependent on the time between post-mortem and chemical skinning as well as the storage conditions (Knight and Trinick, 1982). Furthermore, it is not known what the effect of long-term storage in glycerol has on the fraction and stabilisation of the SRX.

The fraction of myosin in our experiment that occupied the fast hydrolysis population was nearly 80%. It was previously suggested that at any time as 50% of the myosin in the sarcomere would be sequestered in a folded back confirmation like the IHM (Brito *et al.*, 2011) and in relaxed skeletal fibres approximately 50% of the myosin heads occupy the SRX state (Hooijman *et al.*, 2011).

The discrepancy of the fractions of DRX and SRX in our data and the literature may be subject to the experimental temperature. An increase in temperature leads to a higher number of myosin heads to occupy the SRX, extending the ATP lifetimes (Stewart *et al.*, 2010). All our experiments were done at room temperature, and prior to experiments myofibrils were stored either on ice or at 4°C. Using a temperature-controlled optics system would possibly improve the fraction of myosin residing in the SRX. However, this presents a paradox. Higher temperatures increase the number of heads in the SRX but the activity of proteolytic enzymes will likewise increase, which in turn will lead to the breakdown of sarcomeric proteins. Nevertheless, temperature control is a factor to consider for experimental design of future studies.

The binding affinity of ATP should also be considered. The addition of a fluorophore can affect the binding affinity of myosin to the ATP. Previous kinetic studies have shown that MANT-ATP [2′(3′)-O-(A′-methylanthraniloyl)-ATP], a fluorescently tagged ATP analogue, has a high affinity for myosin and behaves similarly as regular ATP (Woodward *et al.*, 1991). The binding affinity of the ATP analogue used in this study, Rhodamine ATP, and if it the activity for actomyosin is comparable to non-fluorescent ATP can be showed by an *in vitro* motility assay.

Another possibility for discrepancy between our results and the expected turnover rates of the two states of relaxed muscle could be due to the off-target use of ATP by non-myosin ATPases in the sarcomere. Does this influence the ATP turnover rate in the myofibril and if so, why is this not apparent from the bulk kinetic studies?

A considerable number of factors therefor remain to be explored. Future studies could also take advantage of the suggested effects of small molecules like mavacamten (Anderson *et al.*, 2018) and phosphorylation of the RLC and MyBP-C on the SRX (Toepfer *et al.*, 2013; McNamara *et al.*, 2016; McNamara *et al.*, 2017; Nag *et al.*, 2017). These proteins have been found of stabilising myosin into the IHM and induce the SRX state of myosin when unphosphorylated. Treating these myofibrils with a suitable kinase will phosphorylate these proteins and all the slow rate constants should be diminished. In cardiac muscle it has been reported that even when partially activated, which induces rapid recruitment of SRX myosin into the DRX in skeletal muscle, there was no change in the fraction of SRX and cross bridges (Hooijman *et al.*, 2011). Comparing single molecule ATP turnover kinetics by cardiac myofibrils with the data we presented here help design future experiments to explain this inconsistency. Is the extra N-terminal domain of cMyBP-C responsible for this or is there another factor that plays a pivotal role in cardiac muscle?

5.3 Presumed location of slower rate in the C-zone

The MyBP-C is an accessory protein of the thick filament located at the C-zone that has been extensively linked the SRX and the IHM (Seiler *et al.*, 1996; Stelzer *et al.*, 2006; McNamara *et al.*, 2015; McNamara *et al.*, 2016; McNamara *et al.*, 2017; Nag *et al.*, 2017). Does this mean that the majority of SRX myosin exist in the C-zone?

STORM reconstruction of the myofibril allowed to explore the spatial arrangement of the occurrence of ATP binding to myosin as well as the average lifetimes. As discussed before, within the A-band there is no regional coinciding between the occurrence and the average lifetime. Closer inspection of the data shows that within the C-zones there is generally a longer lifetime, with fewer ATP binding events. This suggests the primary location of the SRX is in the C-zones and a potential role of MyBP-C.

However, the regional constraints of the A-band and thus of the zones it contains are only suggestive. Due to time constraints we were not able to establish the position of the structural components. Staining the M-lines or Z-lines with fluorescently labelled antibodies, like anti-myomesin with a Q-Dot with a different excitation-emission spectrum than the ATP-fluorophore, would offer a method of labelling the structural components of the sarcomere and subsequently determine the dissociation rate of single molecule ATP on the same sample, without extra complicating steps. Given the spatial resolution we have observed here, it would be valuable to investigate this in future experiments.

6. Conclusion

Research has made great advancements in the understanding of the biochemistry, biophysics and structural organisation of muscle over the last century. It now reached a stage where muscle contraction and the components responsible for this process are fairly well understood. What is less well apprehended however is the molecular basis of diseases that affect the proteins involved in muscle contraction and its regulation. In the last 20 years research in muscle has shifted focus to elucidate this next hurdle of our comprehension of muscle.

The characterisation of two hydrolytic states of ATP turnover by myosin in relaxed conditions has opened new avenues in this understanding. The SRX is a state of myosin with a severely inhibited ATP hydrolysis rate. This may be the result of a structural confirmation of myosin, the IHM, where two adjacent heads are folded back onto the thick filament backbone in a highly ordered arrangement. These states may be regulated by cellular components like the RLC and MyBP-C under the influence of phosphorylation levels or atmospheric changes like stretch force and temperature. In cardiac tissue these relaxed states live in an equilibrium with active state myosin. A shift in this equilibrium is generated by the state of phosphorylation. Mutations that lead to HCM are mapped to the proteins potentially involved with the SRX/IHM.

This study tries to solve the spatiotemporal arrangement of the ATP hydrolysis states and their respective rates at the sarcomeric level. This can be used to further investigate what structural components regulate the SRX. Furthermore, to understand how HCM mutations lead to clinical hyper-contractility, investigations into the functional aspect of the alteration of the intra molecular myosin interactions. Lastly it provides an opportunity of future protein targets that help the development of small molecule effectors for novel therapeutic interventions of HCM.

Ultimately, we show for the first time that it is possible to discern the kinetics of single ATP molecules binding and releasing from myosin in their native myofibrillar environment. The methods described here can be used to further explore the SRX at a single molecule level.

7. References

Ababou, A., Rostkova, E., Mistry, S., Masurier, C. Le, Gautel, M., and Pfuhl, M. (2008) Myosin Binding Protein C Positioned to Play a Key Role in Regulation of Muscle Contraction: Structure and Interactions of Domain C1. *J Mol Biol* **384**: 615–630.

Adhikari, A.S., Kooiker, K.B., Sarkar, S.S., Liu, C., Bernstein, D., Spudich, J.A., and Ruppel, K.M. (2016) Early-Onset Hypertrophic Cardiomyopathy Mutations Significantly Increase the Velocity, Force, and Actin-Activated ATPase Activity of Human β-Cardiac Myosin. *Cell Rep* **17**: 2857–2864.

Ait-Mou, Y., Hsu, K., Farman, G.P., Kumar, M., Greaser, M.L., Irving, T.C., and Tombe, P.P. de (2016) Titin strain contributes to the Frank–Starling law of the heart by structural rearrangements of both thin- and thick-filament proteins. *Proc Natl Acad Sci* **113**: 2306–2311.

Alamo, L., Qi, D., Wriggers, W., Pinto, A., Zhu, J., Bilbao, A., *et al.* (2016) Conserved Intramolecular Interactions Maintain Myosin Interacting-Heads Motifs Explaining Tarantula Muscle Super-Relaxed State Structural Basis. *J Mol Biol* **428**: 1142–1164.

Alamo, L., Wriggers, W., Pinto, A., Bártoli, F., Salazar, L., Zhao, F.Q., *et al.* (2008) Three-Dimensional Reconstruction of Tarantula Myosin Filaments Suggests How Phosphorylation May Regulate Myosin Activity. *J Mol Biol* **384**: 780–797.

Anderson, R.L., Trivedi, D. V., Sarkar, S.S., Henze, M., Ma, W., Gong, H., *et al.* (2018) Deciphering the super relaxed state of human β-cardiac myosin and the mode of action of mavacamten from myosin molecules to muscle fibers. **115**: 8143–8152.

Bailey, K. (1946) Tropomyosin: a New Asymmetric Protein Component of Muscle. *Nature* **157**: 368–369.

Bailey, K. (1948) Tropomyosin: a new asymmetric protein component of the muscle fibril. *Biochem J* **43**: 271 LP – 279.

Bardswell, S.C., Cuello, F., Rowland, A.J., Sadayappan, S., Robbins, J., Gautel, M., *et al.* (2010) Distinct sarcomeric substrates are responsible for protein kinase D-mediated regulation of cardiac myofilament Ca2+sensitivity and cross-bridge cycling. *J Biol Chem* **285**: 5674–5682.

Bates, M., Jones, S.A., and Zhuang, X. (2013) Stochastic optical reconstruction microscopy (STORM): A method for superresolution fluorescence imaging. *Cold Spring Harb Protoc* **8**: 498–520.

Belknap, B., Harris, S.P., and White, H.D. (2014) Modulation of Thin Filament Activation of Myosin ATP Hydrolysis by N-Terminal Domains of Cardiac Myosin Binding Protein-C. *Biochemistry* **53**: 6717–6724.

Brito, R., Alamo, L., Lundberg, U., Guerrero, J.R., Pinto, A., Sulbarán, G., *et al.* (2011) A Molecular Model of Phosphorylation-Based Activation and Potentiation of Tarantula Muscle Thick Filaments. *J Mol Biol* **414**: 44–61.

Burgoyne, T., Morris, E.P., and Luther, P.K. (2015) Three-Dimensional Structure of Vertebrate Muscle Z-Band: The Small-Square Lattice Z-Band in Rat Cardiac Muscle. *J Mol Biol* **427**: 3527–3537.

Buvoli, M., Hamady, M., Leinwand, L.A., and Knight, R. (2008) Bioinformatics Assessment of β-Myosin Mutations Reveals Myosin's High Sensitivity to Mutations. *Trends Cardiovasc Med* **18**: 141–149.

Cheng, Y. (2015) Single-particle Cryo-EM at crystallographic resolution. *Cell* **161**: 450–457.

Colegrave, M., and Peckham, M. (2014) Structural implications of β-cardiac myosin heavy chain mutations in human disease. *Anat Rec* **297**: 1670–1680.

Colson, B.A., Locher, M.R., Bekyarova, T., Patel, J.R., Fitzsimons, D.P., Irving, T.C., and Moss, R.L. (2010) Differential roles of regulatory light chain and myosin binding protein-C phosphorylations in the modulation of cardiac force development. *J Physiol* **588**: 981–993.

Cooke, R. (2011) The role of the myosin ATPase activity in adaptive thermogenesis by skeletal muscle. *Biophys Rev* **3**: 33–45.

Craig, R., Lee, K.H., Mun, J.Y., Torre, I., and Luther, P.K. (2014) Structure, sarcomeric organization, and thin filament binding of cardiac myosin-binding protein-C. *Pflugers Arch Eur J Physiol* **466**: 425–431.

Craig, R., and Offer, G. (1976) The location of C protein in rabbit skeletal muscle. *Proc R Soc London - Biol Sci* **192**: 451–461.

Craig, R., Padron, R., and Kendrick-Jones, J. (1987) Structural changes accompanying phosphorylation of tarantula muscle myosin filaments. *J Cell Biol* **105**: 1319–1327.

Ebashi, S. (1963) Third component participating in the super precipitation of 'natural actomyosin.' *Nature* **200**: 1010.

Ebashi, S., and Endo, M. (1968) Calcium and muscle contraction. *Prog Biophys Mol Biol* **18**: 123–183.

Ebashi, S., Endo, M., and Ohtsuki, I. (1969) Control of muscle contraction. *Q Rev Biophys* **2**: 351–384.

Ferenczi, M.A., Homsher, E., Simmons, R.M., and Trentham, D.R. (1978) Reaction mechanism of the magnesium ion-dependent adenosine triphosphatase of frog muscle myosin and subfragment 1. *Biochem J* **171**: 165–175.

Finer, J.T., Simmons, R.M., and Spudich, J.A. (1994) Single myosin molecule mechanics: piconewton forces and nanometre steps. *Nature* **368**: 113–119.

Flashman, E., Redwood, C., Moolman-Smook, J., and Watkins, H. (2004) Cardiac myosin binding protein C: Its role in physiology and disease. *Circ Res* **94**: 1279–1289.

Freundt, J.K., and Linke, W.A. (2019) Titin as a force-generating muscle protein under regulatory control. *J Appl Physiol* **126**: 1474–1482.

Gautel, M., Zuffardi, O., Freiburg, A., and Labeit, S. (1995) Phosphorylation switches specific for the cardiac isoform of myosin binding protein-C: a modulator of cardiac contraction? *EMBO J* **14**: 1952–1960.

Gebhardt, J.C.M., Suter, D.M., Roy, R., Zhao, Z.W., Chapman, A.R., Basu, S., *et al.* (2013) Single-molecule imaging of transcription factor binding to DNA in live mammalian cells. *Nat Methods* **10**: 421–426.

Geeves, M.A., and Holmes, K.C. (1999) Structural Mechanism of Muscle Contraction. *Annu Rev Biochem* **68**: 687–728.

Geisterfer-Lowrance, A.A., Kass, S., Tanigawa, G., Vosberg, H.P., McKenna, W., Seidman, C.E., Seidman, J.G. (1990) A molecular basis for familial hypertrophic cardiomyopathy: a beta cardiac myosin heavy chain gene missense mutation. *Cell* **62**: 999–1006.

Gruen, M., Prinz, H., and Gautel, M. (1999) cAPK-phosphorylation controls the interaction of the regulatory domain of cardiac myosin binding protein C with myosin-S2 in an on-off fashion. *FEBS Lett* **453**: 254–259.

Hanson, J. (1967) Axial period of actin filaments. *Nature* **213**: 353–356.

Hanson, J., and Lowy, J. (1964) The structure of actin filaments and the origin of the axial periodicity in the I-substance of vertebrate striated muscle. *Proc R Soc London Ser B Biol Sci* **160**: 449–460.

Harris, S.P., Belknap, B., Sciver, R.E. Van, White, H.D., and Galkin, V.E. (2016) C0 and C1 N-terminal Ig domains of myosin binding protein C exert different effects on thin filament activation. *Proc Natl Acad Sci U S A* **113**: 1558–1563.

Harris, S.P., Lyons, R.G., and Bezold, K.L. (2011) In the thick of it: HCM-causing mutations in myosin binding proteins of the thick filament. *Circ Res* **108**: 751–764.

Harvey, P.A., and Leinwand, L.A. (2011) Cellular mechanisms of cardiomyopathy. *J Cell Biol* **194**: 355–365.

Haselgrove, J.C. (1973) X-ray evidence for a conformational change in the actin-containing filaments of vertebrate striated muscle. *Cold Spring Harb Symp Quant Biol* **37**: 341–352.

Heling, L.W.H.J., Geeves, M.A., and Kad, N.M. (2020) MyBP-C: one protein to govern them all. *J Muscle Res Cell Motil* 1–11.

Homburger, J.R., Green, E.M., Caleshu, C., Sunitha, M.S., Taylor, R.E., Ruppel, K.M., *et al.* (2016) Multidimensional structure-function relationships in human β-cardiac myosin from population-scale genetic variation. *Proc Natl Acad Sci* **113**: 6701–6706.

Hooijman, P., Stewart, M.A.A., and Cooke, R. (2011) A new state of cardiac myosin with very slow ATP turnover: A potential cardioprotective mechanism in the heart. *Biophys J* **100**: 1969–1976.

Hu, L.-Y.R., Ackermann, M.A., and Kontrogianni-Konstantopoulos, A. (2015) The sarcomeric M-region: A molecular command center for diverse cellular processes. *Biomed Res Int* 1–26.

Huxley, A.F., and Niedergerke, R. (1954) Structural changes in muscle during contraction: interference microscopy of living muscle fibres. *Nature* **173**: 971.

Huxley, H.E. (1953a) Electron microscope studies of the organisation of the filaments in striated muscle. *Biochim Biophys Acta* **12**: 387–394.

Huxley, H.E. (1953b) X-ray analysis and the problem of muscle. *Proc R Soc London Ser B-Biological Sci* **141**: 59–62.

Huxley, H.E. (1957) The double array of filaments in cross-striated muscle. *J Cell Biol* **3**: 631–648.

Huxley, H.E. (1969) The mechanism of muscular contraction. *Science (80-)* **164**: 1356–65.

Huxley, H.E. (1971) Structural changes during muscle contraction. *Biochem J* **125**: 85.

Huxley, H.E., and Hanson, J. (1954) Changes in the Cross-Striations of Muscle during Contraction and Stretch and their Structural Interpretation. *Nature* **173**: 973.

Inchingolo, A. V., Previs, S.B., Previs, M.J., Warshaw, D.M., and Kad, N.M. (2019) Revealing the mechanism of how cardiac myosin-binding protein C N-terminal fragments sensitize thin filaments for myosin binding. *Proc Natl Acad Sci U S A* **116**: 6828–6835.

Irving, M. (2017) Regulation of Contraction by the Thick Filaments in Skeletal Muscle. **113**: 2579–2594.

Kad, N.M., Kim, S., Warshaw, D.M., VanBuren, P., and Baker, J.E. (2005) Single-myosin crossbridge interactions with actin filaments regulated by troponin-tropomyosin. *Proc Natl*

Acad Sci U S A **102**: 16990–16995.

Kampourakis, T., and Irving, M. (2015) Phosphorylation of myosin regulatory light chain controls myosin head conformation in cardiac muscle. *J Mol Cell Cardiol* **85**: 199–206.

Kawana, M., Sarkar, S.S., Sutton, S., Ruppel, K.M., and Spudich, J.A. (2017) Biophysical properties of human b-cardiac myosin with converter mutations that cause hypertrophic cardiomyopathy. *Sci Adv* **3**: 1–10.

Kensler, R.W., and Harris, S.P. (2008) The structure of isolated cardiac myosin thick filaments from cardiac myosin binding protein-C knockout mice. *Biophys J* **94**: 1707–1718.

Kensler, R.W., Shaffer, J.F., and Harris, S.P. (2011) Binding of the N-terminal fragment C0-C2 of cardiac MyBP-C to cardiac F-actin. *J Struct Biol* **174**: 44–51.

Knight, P.J., and Trinick, J.A. (1982) Preparation of Myofibrils. *Methods Enzymol* **85**: 9–12.

Knöll, R., Buyandelger, B., and Lab, M. (2011) The sarcomeric Z-disc and Z-discopathies. *J Biomed Biotechnol* 1–12.

Kobirumaki-Shimozawa, F., Inoue, T., Shintani, S.A., Oyama, K., Terui, T., Minamisawa, S., *et al.* (2014) Cardiac thin filament regulation and the Frank-Starling mechanism. *J Physiol Sci* **64**: 221–232.

Koebis, M., Ohsawa, N., Kino, Y., Sasagawa, N., Nishino, I., and Ishiura, S. (2011) Alternative splicing of myomesin 1 gene is aberrantly regulated in myotonic dystrophy type 1. *Genes to Cells* **16**: 961–972.

Kron, S.J., and Spudich, J.A. (1986) Fluorescent actin filaments move on myosin fixed to a glass surface. *Proc Natl Acad Sci* **83**: 6272–6276.

Kühne, W.F. (1864) *Untersuchungen über das Protoplasma und die Contractilität*. W. Engelmann, Leipzig.

Lange, S., Pinotsis, N., Agarkova, I., and Ehler, E. (2019) The M-band: The underestimated part of the sarcomere. *Biochim Biophys Acta - Mol Cell Res* 1–11.

Lehrer, S.S., and Morris, E.P. (1982) Dual effects of tropomyosin and troponin-tropomyosin on actomyosin subfragment 1 ATPase. *J Biol Chem* **257**: 8073–8080.

Levine, R.J., Kensler, R.W., Yang, Z., Stull, J.T., and Sweeney, H.L. (1996) Myosin light chain phosphorylation affects the structure of rabbit skeletal muscle thick filaments. *Biophys J* **71**: 898–907.

Li, G.W., and Xie, X.S. (2011) Central dogma at the single-molecule level in living cells. *Nature* **475**: 308–315.

Linari, M., Brunello, E., Reconditi, M., Fusi, L., Caremani, M., Narayanan, T., *et al.* (2015) Force generation by skeletal muscle is controlled by mechanosensing in myosin filaments. *Nature* **528**: 276–279.

Lowey, S., and Trybus, K.M. (2010) Common structural motifs for the regulation of divergent class II myosins. *J Biol Chem* **285**: 16403–16407.

Lowey, S., Waller, G.S., and Trybus, K.M. (1993) Skeletal muscle myosin light chains are essential for physiological speeds of shortening. *Nature* **365**: 454–456.

Lu, Y., Kwan, A.H., Trewhella, J., and Jeffries, C.M. (2011) The C0C1 fragment of human cardiac myosin binding protein C has common binding determinants for both actin and myosin. *J Mol Biol* **413**: 908–913.

Luther, P.K. (2009) The vertebrate muscle Z-disc: Sarcomere anchor for structure and signalling. *J Muscle Res Cell Motil* **30**: 171–185.

Luther, P.K., Winkler, H., Taylor, K., Zoghbi, M.E., Craig, R., Padron, R., *et al.* (2011) Direct visualization of myosin-binding protein C bridging myosin and actin filaments in intact muscle. *Proc Natl Acad Sci* **108**: 11423–11428.

Lymn, R.W., and Taylor, E.W. (1971) Mechanism of Adenosine Triphosphate Hydrolysis by Actomyosin. *Biochemistry* **10**: 4617–4624.

Malik, F.I., Hartman, J.J., Elias, K.A., Morgan, B.P., Rodriguez, H., Brejc, K., *et al.* (2011) Cardiac myosin activation: A potential therapeutic approach for systolic heart failure. *Science (80-)* **331**: 1439–1443.

Maron, B.J., Maron, M.S., and Maron, B.J. (2013) Hypertrophic cardiomyopathy. *Lancet* **381**: 242–55.

Maruyama, K., and Ebashi, S. (1965) α-actinin, a new structural protein from striated muscle: II. action on actin. *J Biochem* **58**: 13–19.

Maytum, R., Lehrer, S.S., and Geeves, M.A. (1999) Cooperativity and switching within the three-state model of muscle regulation. *Biochemistry* **38**: 1102–1110.

McKenna, W.J., and Behr, E.R. (2002) Hypertrophic cardiomyopathy: management, risk stratification, and prevention of sudden death. *Heart* **87**: 169–176.

Mckillop, D.F.A., and Geeves, M.A. (1993) Regulation of the Interaction between Actin and Myosin Subfragment 1: Evidence for Three States of the Thin Filament. *Biophys J Vol* **65**: 693–701.

McNamara, J.W., Li, A., Lal, S., Bos, J.M., Harris, S.P., Velden, J. Van Der, *et al.* (2017) MYBPC3 mutations are associated with a reduced super-relaxed state in patients with hypertrophic cardiomyopathy. *PLoS One* **12**: 1–22.

McNamara, J.W., Li, A., Remedios, C.G. dos, and Cooke, R. (2015) The role of super-relaxed myosin in skeletal and cardiac muscle. *Biophys Rev* **7**: 5–14.

McNamara, J.W., Li, A., Smith, N.J., Lal, S., Graham, R.M., Kooiker, K.B., *et al.* (2016) Ablation of cardiac myosin binding protein-C disrupts the super-relaxed state of myosin in murine cardiomyocytes. *J Mol Cell Cardiol* **94**: 65–71.

Mohamed, A.S., Dignam, J.D., and Schlender, K.K. (1998) Cardiac myosin-binding protein C (MyBP-C): Identification of protein kinase A and protein kinase C phosphorylation sites. *Arch Biochem Biophys* **358**: 313–319.

Moos, C., Mason, C.M., Besterman, J.M., Feng, I.N.M., and Dubin, J.H. (1978) The binding of skeletal muscle C-protein to F-actin, and its relation to the interaction of actin with myosin subfragment-1. *J Mol Biol* **124**: 571–586.

Mun, J.Y., Gulick, J., Robbins, J., Woodhead, J., Lehman, W., and Craig, R. (2011) Electron microscopy and 3D reconstruction of F-actin decorated with cardiac myosin-binding protein

C (cMyBP-C). *J Mol Biol* **410**: 214–225.

Mun, J.Y., Previs, M.J., Yu, H.Y., Gulick, J., Tobacman, L.S., Beck Previs, S., *et al.* (2014) Myosin-binding protein C displaces tropomyosin to activate cardiac thin filaments and governs their speed by an independent mechanism. *Proc Natl Acad Sci* **111**: 2170–2175.

Myburgh, K.H., Franks-Skiba, K., and Cooke, R. (1995) Nucleotide turnover rate measured in fully relaxed rabbit skeletal muscle myofibrils. *J Gen Physiol* **106**: 957–973.

Naber, N., Cooke, R., and Pate, E. (2011) Slow Myosin ATP Turnover in the Super-Relaxed State in Tarantula Muscle. *J Mol Biol* **411**: 943–950.

Nag, S., Sommese, R.F., Ujfalusi, Z., Combs, A., Langer, S., Sutton, S., *et al.* (2015) Contractility parameters of human b-cardiac myosin with the hypertrophic cardiomyopathy mutation R403Q show loss of motor function. *Sci Adv* **1**: 1–17.

Nag, S., Trivedi, D. V., Sarkar, S.S., Adhikari, A.S., Sunitha, M.S., Sutton, S., *et al.* (2017) The myosin mesa and the basis of hypercontractility caused by hypertrophic cardiomyopathy mutations. *Nat Struct Mol Biol* **24**: 525–533.

Ngai, P.K., Groschel-Stewart, U., and Walsh, M.P. (1986) Comparison of the effects of smooth and skeletal muscle actins on smooth muscle actomyosin Mg2+-atpase. *Biochem Int* **12**: 89–93.

Nogales, E., and Scheres, S.H.W. (2015) Cryo-EM: A Unique Tool for the Visualization of Macromolecular Complexity. *Mol Cell* **58**: 677–689.

Orlova, A., Galkin, V.E., Jeffries, C.M.J., Egelman, E.H., and Trewhella, J. (2011) The N-terminal domains of myosin binding protein C can bind polymorphically to F-actin. *J Mol Biol* **412**: 379–386.

Padrón, R., Panté, N., Sosa, H., and Kendrick-Jones, J. (1991) X-ray diffraction study of the structural changes accompanying phosphorylation of tarantula muscle. *J Muscle Res Cell Motil* **12**: 235–241.

Parry, D.A.D., and Squire, J.M. (1973) Structural role of tropomyosin in muscle regulation: Analysis of the X-ray diffraction patterns from relaxed and contracting muscles. *J Mol Biol* **75**: 33–

55.

Poole, K.J. V, Lorenz, M., Evans, G., Rosenbaum, G., Pirani, A., Craig, R., *et al.* (2006) A comparison of muscle thin filament models obtained from electron microscopy reconstructions and low-angle X-ray fibre diagrams from non-overlap muscle. *J Struct Biol* **155**: 273–284.

Potter, J.D. (1974) The content of troponin, tropomyosin, actin, and myosin in rabbit skeletal muscle myofibrils. *Arch Biochem Biophys* **162**: 436–441.

Previs, M.J., Previs, S.B., Gulick, J., Robbins, J., Warshaw, D.M., Beck Previs, S., *et al.* (2012) Molecular Mechanics of Cardiac Myosin-Binding Protein C in Native Thick Filaments. *Science (80-)* **337**: 1215–1218.

Ratti, J., Rostkova, E., Gautel, M., and Pfuhl, M. (2011) Structure and interactions of myosin-binding protein C domain C0: Cardiac-specific regulation of myosin at its neck? *J Biol Chem* **286**: 12650–12658.

Razumova, M. V., Shaffer, J.F., Tu, A.Y., Flint, G. V., Regnier, M., and Harris, S.P. (2006) Effects of the N-terminal domains of myosin binding protein-C in an in vitro motility assay: Evidence for long-lived cross-bridges. *J Biol Chem* **281**: 35846–35854.

Reconditi, M., Caremani, M., Pinzauti, F., Powers, J.D., Narayanan, T., Stienen, G.J.M., *et al.* (2017) Myosin filament activation in the heart is tuned to the mechanical task. *Proc Natl Acad Sci U S A* **114**: 3240–3245.

Risi, C., Belknap, B., Forgacs-Lonart, E., Harris, S.P., Schröder, G.F., White, H.D., and Galkin, V.E. (2018) N-Terminal Domains of Cardiac Myosin Binding Protein C Cooperatively Activate the Thin Filament. *Structure* **26**: 1604–1611.

Saber, W., Begin, K.J., Warshaw, D.M., and VanBuren, P. (2008) Cardiac myosin binding protein-C modulates actomyosin binding and kinetics in the in vitro motility assay. *J Mol Cell Cardiol* **44**: 1053–1061.

Sadayappan, S., Gulick, J., Osinska, H., Martin, L.A., Hahn, H.S., Dorn, G.W., *et al.* (2005) Cardiac myosin-binding protein-C phosphorylation and cardiac function. *Circ Res* **97**: 1156–1163.

Schindelin, J., Arganda-Carreras, I., Frise, E., Kaynig, V., Longair, M., Pietzsch, T., *et al.* (2012) Fiji: an open-source platform for biological-image analysis. *Nat Methods* **9**: 676.

Scruggs, S.B., Hinken, A.C., Thawornkaiwong, A., Robbins, J., Walker, L.A., Tombe, P.P. de, *et al.* (2009) Ablation of ventricular myosin regulatory light chain phosphorylation in mice causes cardiac dysfunction in situ and affects neighboring myofilament protein phosphorylation. *J Biol Chem* **284**: 5097–5106.

Seidman, J.G., and Seidman, C. (2001) The genetic basis for cardiomyopathy: From mutation identification to mechanistic paradigms. *Cell* **104**: 557–567.

Seiler, S.H., Fischman, D.A., and Leinwand, L.A. (1996) Modulation of myosin filament organization by C-protein family members. *MolBiolCell* **7**: 113–127.

Selby, C.C., and Bear, R.S. (1956) The structure of actin-rich filaments of muscles according to x-ray diffraction. *J Biophys Biochem Cytol* **2**: 71–85.

Semsarian, C., Ingles, J., Maron, M.S., and Maron, B.J. (2015) New Perspectives on the Prevalence of Hypertrophic Cardiomyopathy. *J Am Coll Cardiol* **65**: 1249–1254.

Siegert, R., Perrot, A., Keller, S., Behlke, J., Michalewska-Włudarczyk, A., Wycisk, A., *et al.* (2011) A myomesin mutation associated with hypertrophic cardiomyopathy deteriorates dimerisation properties. *Biochem Biophys Res Commun* **405**: 473–479.

Sommese, R.F., Sung, J., Nag, S., Sutton, S., Deacon, J.C., Choe, E., *et al.* (2013) Molecular consequences of the R453C hypertrophic cardiomyopathy mutation on human β-cardiac myosin motor function. *Proc Natl Acad Sci U S A* **110**: 12607–12612.

Springall, L., Inchingolo, A. V., and Kad, N.M. (2016) DNA-protein interactions studied directly using single molecule fluorescence imaging of quantum dot tagged proteins moving on DNA tightropes. In *Methods in Molecular Biology*. pp. 141–150.

Starr, R., and Offer, G. (1971) Polypeptide chains of intermediate molecular weight in myosin preparations. *FEBS Lett* **15**: 40–44.

Stelzer, J.E., Fitzsimons, D.P., and Moss, R.L. (2006) Ablation of myosin-binding protein-C accelerates force development in mouse myocardium. *Biophys J* **90**: 4119–4127.

Stewart, M.A., Franks-Skiba, K., Chen, S., and Cooke, R. (2010) Myosin ATP turnover rate is a mechanism involved in thermogenesis in resting skeletal muscle fibers. *Proc Natl Acad Sci* **107**: 430–435.

Stringham, J.C., Southard, J.H., Hegge, J., Triemstra, L., Fields, B.L., and Belzer, F.O. (1992) Limitations of Heart Preservation By Cold Storage. *Transplantation* **53**: 287–294.

Szczesna, D., Ghosh, D., Li, Q., Gomes, A. V., Guzman, G., Arana, C., *et al.* (2001) Familial Hypertrophic Cardiomyopathy Mutations in the Regulatory Light Chains of Myosin Affect their Structure, Ca2+ Binding, and Phosphorylation. *J Biol Chem* **276**: 7086–7092.

Szent-Györgyi, A. (1951) *Chemistry of Muscular Contraction*. 2nd ed., Academic Press Inc., New York.

Tinevez, J.-Y., Perry, N., Schindelin, J., Hoopes, G.M., Reynolds, G.D., Laplantine, E., *et al.* (2017) TrackMate: An open and extensible platform for single-particle tracking. *Methods* **115**: 80–90.

Toepfer, C., Caorsi, V., Kampourakis, T., Sikkel, M.B., West, T.G., Leung, M.C., *et al.* (2013) Myosin regulatory light chain (RLC) phosphorylation change as a modulator of cardiac muscle contraction in disease. *J Biol Chem* **288**: 13446–13454.

Tokunaga, M., Imamoto, N., and Sakata-Sogawa, K. (2008) Highly inclined thin illumination enables clear single-molecule imaging in cells. *Nat Methods* **5**: 159–161.

Towbin, J.A. (2009) Hypertrophic Cardiomyopathy. *Pacing Clin Electrophysiol* **32**: S23–S31.

Toyoshima, Y.Y., Kron, S.J., McNally, E.M., Niebling, K.R., Toyoshima, C., and Spudich, J.A. (1987) Myosin subfragment-1 is sufficient to move actin filaments in vitro. *Nature* **328**: 536–539.

Trinick, J. (1996) Cytoskeleton: Titin as a scaffold and spring. *Curr Biol* **6**: 258–260.

Trivedi, D. V., Adhikari, A.S., Sarkar, S.S., Ruppel, K.M., and Spudich, J.A. (2017) Hypertrophic cardiomyopathy and the myosin mesa: viewing an old disease in a new light. *Biophys Rev* **10**: 1–22.

Trybus, K.M., Freyzon, Y., Faust, L.Z., and Sweeney, H.L. (1997) Spare the rod, spoil the regulation: Necessity for a myosin rod. *Proc Natl Acad Sci U S A* **94**: 48–52.

Ujfalusi, Z., Vera, C.D., Mijailovich, S.M., Svicevic, M., Yu, E.C., Kawana, M., *et al.* (2018) Dilated cardiomyopathy myosin mutants have reduced force-generating capacity. *J Biol Chem* **293**: 9017–9029.

Vibert, P., Craig, R., and Lehman, W. (1997) Steric-model for activation of muscle thin filaments. *J Mol Biol* **266**: 8–14.

Walcott, S., Docken, S., and Harris, S.P. (2015) Effects of Cardiac Myosin Binding Protein-C on Actin Motility Are Explained with a Drag-Activation-Competition Model. *Biophys J* **108**: 10–13.

Walsh, R., Rutland, C., Thomas, R., and Loughna, S. (2009) Cardiomyopathy: A systematic review of disease-causing mutations in myosin heavy chain 7 and their phenotypic manifestations. *Cardiology* **115**: 49–60.

Wendt, T., Taylor, D., Messier, T., Trybus, K.M., and Taylor, K.A. (1999) Visualization of head-head interactions in the inhibited state of smooth muscle myosin. *J Cell Biol* **147**: 1385–1390.

Whitten, A.E., Jeffries, C.M., Harris, S.P., and Trewhella, J. (2008) Cardiac myosin-binding protein C decorates F-actin: Implications for cardiac function. *Proc Natl Acad Sci* **105**: 18360–18365.

Wood, D.S., Zollman, J., Reuben, J.P., and Brandt, P.W. (1975) Human skeletal muscle: Properties of the “chemically skinned” fiber. *Science (80-)* **187**: 1075–1076.

Woodhead, J.L., Zhao, F.Q., Craig, R., Egelman, E.H., Alamo, L., and Padrón, R. (2005) Atomic model of a myosin filament in the relaxed state. *Nature* **436**: 1195–1199.

Woodward, S.K.A., Eccleston, J.F., and Geeves, M.A. (1991) Kinetics of the interaction of 2’(3’)-

O-(N-methylanthraniloyl)-ATP with myosin subfragment 1 and actomyosin subfragment 1: Characterization of two acto.cntdot.S1.cntdot.ADP complexes. *Biochemistry* **30**: 422–430.

World Health Organisation (2018) Overweight and obesity. https://www.who.int/gho/ncd/risk_factors/overweight/en/. Accessed August 2, 2019.

Yasuda, M., Koshida, S., Sato, N., and Obinata, T. (1995) Complete primary structure of chicken cardiac C-protein (MyBP-C) and its expression in developing striated muscles. *J Mol Cell Cardiol* **27**: 2275–2286.

Zhao, F.Q., Craig, R., and Woodhead, J.L. (2009) Head-Head Interaction Characterizes the Relaxed State of Limulus Muscle Myosin Filaments. *J Mol Biol* **385**: 423–431.

Zoghbi, M.E., Woodhead, J.L., Moss, R.L., and Craig, R. (2008) Three-dimensional structure of vertebrate cardiac muscle myosin filaments. *Proc Natl Acad Sci U S A* **105**: 2386–90.

Zurlo, F., Larson, K., Bogardus, C., and Ravussin, E. (1990) Skeletal muscle metabolism is a major determinant of resting energy expenditure. *J Clin Invest* **86**: 1423–1427.